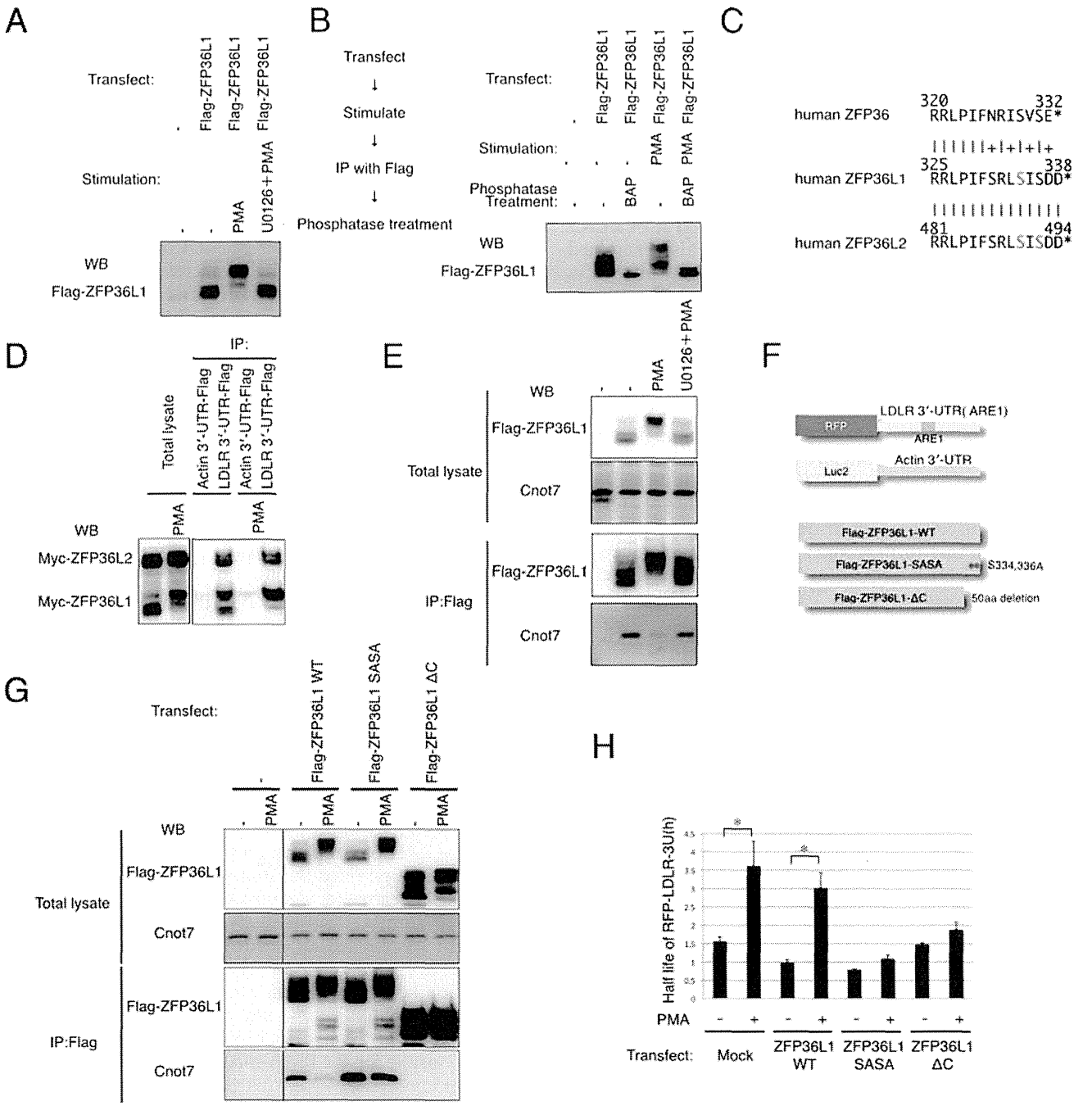

Figure 4. ERK pathway phosphorylates and inhibits ZFP36L2. (**A**) 293T cells were transfected with Flag-tagged ZFP36L1. Twenty-four hours after transfection, cells were treated with PMA (for 30 min) and U0126 (for 45 min), as indicated. Cell lysates were subjected to western blot analysis using anti-Flag antibody. (**B**) 293T cells were transfected with Flag-tagged ZFP36L1. Cells were treated with or without PMA (for 30 min) and the lysates were subjected to IP. Immunopurified Flag-ZFP36L1 was treated with or without bacterial acid phosphatase (BAP) and samples were subjected to western blot analysis using anti-Flag antibody. (**C**) Alignment of C-terminal amino acid sequences in the human ZFP36 family. The C-terminal end of each protein is shown as (*). Identical residues are shown by (l) and similar residues are shown by (+). The serine residues identified as being phosphorylated downstream of ERK are shown in red. (**D**) 293T cells were transfected with Myc-tagged ZFP36L1 or ZFP36L2 and then treated with or without PMA (for 30 min). Cell lysates were subjected to IP using the Flag-antibody and the indicated bait RNAs. Co-immunoprecipitated proteins were subjected to western blot analysis using anti-MYC (9E10) antibody. (**E**) 293T cells were transfected with Flag-tagged ZFP36L1, then treated with PMA (for 30 min) and U0126 (for 45 min) as indicated, and lysates were subjected to IP. Co-immunoprecipitated proteins were subjected to western blot analysis using the indicated antibodies. (**F**) Schematic representation of the constructs used in this experiment. (**G**) 293T cells were transfected with the indicated constructs. Twenty-four hours after transfection, cells were treated with or without PMA (for 30 min), and lysates were subjected to IP. Co-immunoprecipitated proteins were subjected to western blot analysis using the indicated antibodies. (**H**) HeLa cells were transfected with RFP-LDLR 3′-UTR (ARE1) or Luc2-β-Actin-UTR along with the indicated ZFP36L1 constructs. Twenty-four hours after transfection, cells were treated with ActD and PMA (PMA treatment commenced 15 min after ActD treatment), as indicated. Two hours after ActD treatment, cells were harvested and total RNA was extracted. Quantitative RT-PCR (qPCR) was performed using RFP and Luc2-specific primers. Results were normalized to the levels of Luc2 mRNA. The data are representative of at least three independent experiments.

WT, ZFP36L1-SASA or ZFP36L1-ΔC into 293T cells and preformed ActD chase experiments with or without PMA treatment. We observed PMA-mediated stabilization of RFP-LDLR-3′-UTR in mock- and wild-type-ZFP36L1-transfected cells, but not in ZFP36L1-SASA or ZFP36L1-ΔC mutant-transfected cells (Figure 4F and H). These results indicate that ZFP36L1 is regulated by PMA, and that C-terminal phosphorylation of ZFP36L1 is indispensable for ERK-mediated LDLR-mRNA stabilization.

RSK directly phosphorylates ZFP36L1 downstream of ERK

We showed that the C-terminal serine-334 of ZFP36L1 and the C-terminal serine-493 and -495 of ZFP36L2 are phosphorylated downstream of ERK. However, these sites do not match the consensus MAP kinase recognition motifs (SP or TP), indicating that ERK does not directly phosphorylate ZFP36L1. We then examined the possibility that RSK, a major downstream kinase of ERK, directly phosphorylates the C-terminus of ZFP36L1. We first investigated whether BI-D1870 and SL0101, established RSK inhibitors, can reverse PMA-mediated dissociation between ZFP36L1 and CNOT7 protein. We found that BI-D1870 and SL0101 clearly reversed the effect of PMA (Figure 5A, Supplementary Figure S6A). We then examined whether RSK1 directly phosphorylates the C-terminus of ZFP36L1 using recombinant proteins. We incubated *E. coli*-expressed GST-ZFP36L1 with or without active recombinant RSK1 protein under phosphorylation conditions, and analyzed the C-terminal phosphorylation of GST-ZFP36L1 by MS. We found that the C-terminal serine-334 of ZFP36L1 is phosphorylated only when we incubated GST-ZFP36L1 with active RSK1 (Figure 5B and C, Supplementary Figure S6B). We also examined whether active RSK1 inhibits the ability of ZFP36L1 to interact with CNOT proteins. We incubated GST-ZFP36L1 protein with mock buffer, active recombinant ERK1 and/or active recombinant RSK1 under phosphorylation conditions, washed out residual kinase, added 293T cell lysate and performed pulldowns with glutathione-sepharose. We found that GST-ZFP36L1 looses its ability to interact with CNOT1 and CNOT7 proteins when incubated with active recombinant RSK1 (Figure 5D). These results indicate that RSK1 directly phosphorylates the C-terminus of ZFP36L1 downstream of ERK, and inhibits the mRNA destabilization activity of ZFP36L1.

To further confirm our finding that ZFP36L1 and ZFP36L2 are inhibited by PMA treatment, we examined the effect of PMA on the stability of polo-like kinase 3 (PLK3), VEGFA and cellular myelocytomatosis oncogene (cMYC) mRNAs. PLK3 and VEGFA mRNAs have recently been identified as targets of ZFP36L1 (7,8), whereas cMYC mRNA does not bind to ZFP36L1 or ZFP36L2. We found that PLK3 and VEGFA mRNAs were also stabilized by PMA, but that this was not the case for cMYC mRNA (Supplementary Figure S7). These data strongly support the regulation of ZFP36 family proteins by PMA.

DISCUSSION

We have identified ZFP36L1 and ZFP36L2 as two proteins that specifically interact with LDLR mRNA. We showed that ZFP36L1 and ZFP36L2 destabilize LDLR mRNA and that this activity is inhibited by ERK/RSK1 signaling. Recently, KHSRP, hnRNPD and PTBP1 have been reported to be LDLR-destabilizing proteins (5). However, using our approach, we identified KHSRP as a binding protein for the 3′-UTRs of IFNA1, β-actin and cMYC mRNAs and hnRNPD and PTBP1 were common to all the RNA baits. In spite of the binding of these proteins, IFNA1 and β-actin mRNAs were stable, whereas cMYC mRNA was unstable and was not stabilized by ERK signaling. How these proteins selectively regulate the stability of LDLR mRNA is unclear. It is possible that ZFP36L1 and ZFP36L2 coordinately regulate the stability of LDLR mRNA along with KHSRP, hnRNPD and PTBP1.

Target prediction of ZFP36L1 and ZFP36L2

ZFP36L1 and ZFP36L2 belong to the family of CCCH tandem zinc finger proteins (the ZFP36 family), members of which interact with AREs containing a UAUU-UAUU sequence and trigger the degradation of several ARE-containing mRNAs, including PLK3 and VEGFA (7,8,18,19). Consistent with previous reports, we found that ZFP36L1 and ZFP36L2 predominantly interact with the UAUUUAUU sequence of the ARE1 region of the LDLR mRNA, even though the ARE2 region of the LDLR mRNA also contains the same sequence. Interestingly, IFNA1 mRNA, which also has a UAUUUAUU sequence in its 3′-UTR, is stable in cells and ZFP36L1 does not interact strongly with the 3′-UTR of this mRNA (Figure 1B, Supplementary Table S2). Our results suggest that the UAUUUAUU sequence is necessary but not sufficient for ZFP36L1 and ZFP36L2 to interact with and destabilize mRNA. Further investigation is required to predict the target mRNAs of ZFP36L1 and ZFP36L2 *in silico*.

Methods used to identify the regulator of RNA stability

The methods used for (RBP) purification are generally classified into *in vivo* and *in vitro* categories. The *in vivo* purification approach makes use of antisense oligonucleotides, aptamers or MS2-based purification to identify interactions between RNA and RBPs within cells (13,20–24). Use of these methods has elucidated important information on interactions (22–24). On the other hand, the *in vitro* purification approach makes use of cell lysates to purify and identify proteins interacting with *in vitro* synthesized RNA. It is known that some critical regulators of specific RNAs interact specifically with RNA *in vitro* (25). The *in vitro* purification method has several advantages. First, since experimental mRNA expression in cells is not required, this method is sufficiently flexible to enable a wide variety of cells to be used without concerns for transfection efficiency or mRNA expression levels. Second, the amount of bait RNA to be used can be precisely determined to obtain reproducible results that can be subjected to comparison analysis. Third, it is possible to use the RNA sequence of interest, which reduces the amount of nonspecific protein interactions, e.g. with ribosomal proteins or PABPs. Given these advantages, plus our fully automated robotic IP and protein identification system, which is highly sensitive and reproducible (11),

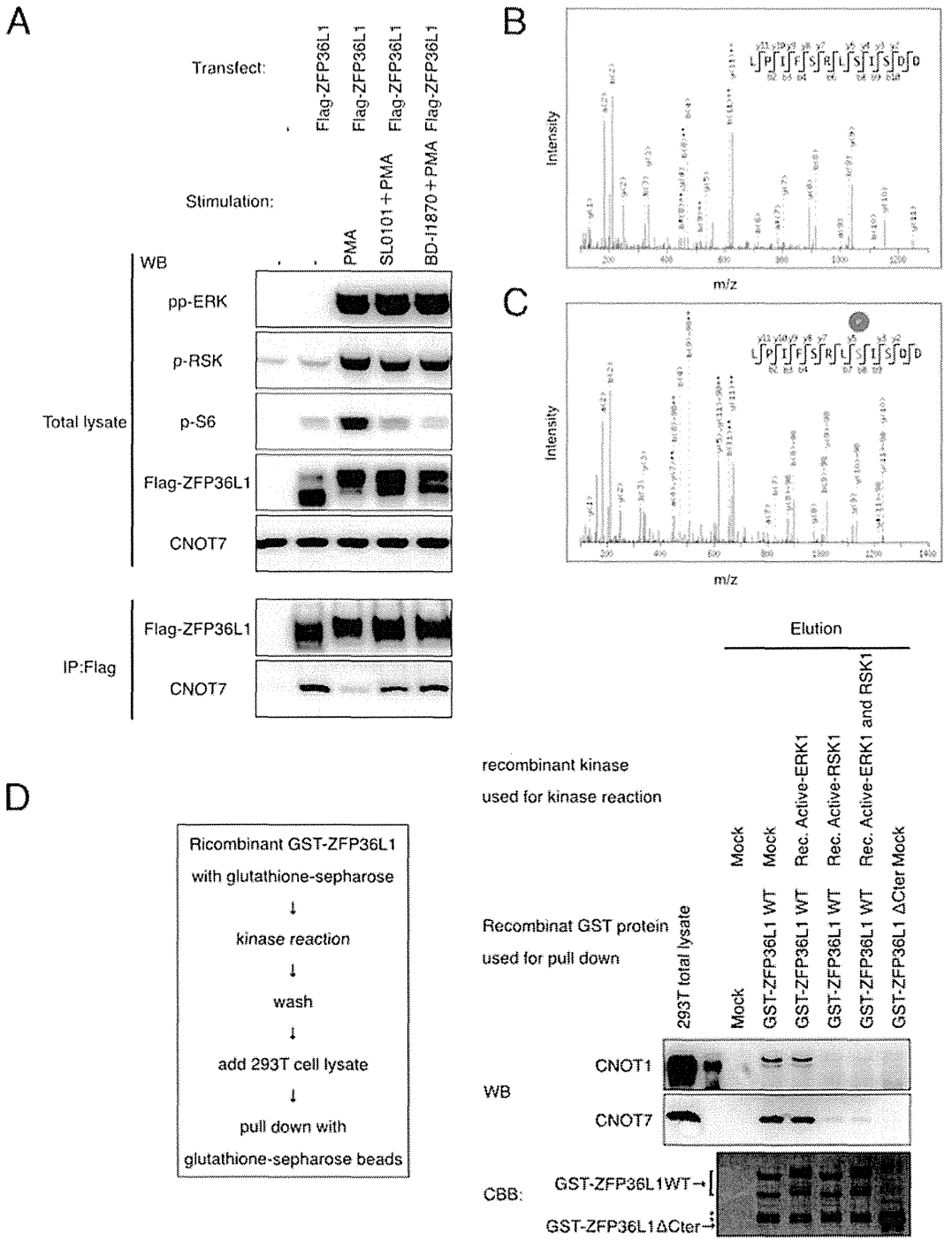

Figure 5. RSK1 directly phosphorylates the C-terminus of ZFP36L1. (**A**) 293T cells were transfected with Flag-tagged ZFP36L1. Twenty-four hours after transfection, cells were treated with PMA (for 30 min) and BI-D1870 or SL0101 (for 45 min) as indicated, and lysates were subjected to IP with the anti-Flag antibody. Co-immunoprecipitated proteins were subjected to western blot analysis using the indicated antibodies. Five percent of the initial amount of cleared 293T lysate was loaded as total lysate. (**B**) GST-ZFP36L1 protein was incubated with or without active recombinant RSK1 under phosphorylation conditions for 30 min. Phosphorylation of GST-ZFP36L1 C-terminal peptide was analyzed by MS. The MS/MS spectrum used to identify the m/z 681.8604-peak as the LPIFSRLSISDD peptide fragment of ZFP36L1 is shown. (**C**) MS/MS spectrum used to identify the m/z 721.8421-peak as the serine-8 phosphorylated LPIFSRLSISDD peptide fragment of ZFP36L1. (**D**) GST-ZFP36L1 protein was incubated with the indicated recombinant kinase under phosphorylation conditions for 30 min, washed, then added to 293T cell lysate and then subjected to pulldown with glutathione-sepharose. Eluted proteins were subjected to western blot analysis using the indicated antibodies and subjected to Coomassie Brilliant Blue (CBB) staining. The asterisk shows a nonspecific band. Five percent of the initial amount of cleared 293T cell lysate was loaded as total lysate. These data are representative of at least three independent experiments.

we opted to use the *in vitro* purification approach, combined with comparison analysis. This allowed us to demonstrate that ZFP36L1 and ZFP36L2 specifically interact with LDLR mRNA, leading to its destabilization. We also identified several known interactions with other bait RNAs including 7SK-CDK9 and 7SK-LARP7. Thus, our results demonstrate that our *in vitro* purification approach is useful for identifying critical regulators of RNAs, which may be used in the identification of important regulators of other types of RNA.

Oligonucleotide-based functional validation

We used RNAi-based knockdown to assess the function of ZRP36L1 and ZFP36L2, but as with many RNA-regulating proteins, ZFP36L1 and ZFP36L2 regulate multiple target mRNAs (6). This makes it difficult to determine whether the result of knockdown is directly caused by inhibition of the interaction between the mRNA and the putative regulator, or is a secondary effect. We therefore performed targeted disruption of the interaction between LDLR-mRNA and ZFP36L1 and ZFP36L2 proteins, using LNA- (9) modified antisense oligonucleotides. LNA is a new-generation artificial nucleotide involving a 2′- and 4′-linked ribose moiety. LNA oligonucleotides have several useful characteristics (26): (i) LNA oligonucleotides are resistant to exo- and endonucleases; (ii) LNA oligonucleotides do not evoke RNase H activity when paired with a complementary RNA strand; (iii) LNA oligonucleotides have very high specificity for complementary RNA and can discriminate even a single-base difference; therefore, short oligonucleotides can be used. Thus, we used LNA-modified antisense oligonucleotides to disrupt the interaction between LDLR and ZFP36L1 and ZFP36L2.

A crucial factor in using antisense-oligonucleotides for such a purpose is to show that the effect of the antisense-oligonucleotide is caused by the interaction between the antisense-oligonucleotide and the intended target mRNA. We have shown several lines of evidence to confirm that the effect of the antisense-oligonucleotide (Oligo-L1) was caused by disrupting the interaction between LDLR mRNA and ZFP36L1 and ZFP36L2: (i) Oligo-L1 could inhibit the interaction between ZFP36L1 and LRLD mRNA, without affecting the interaction between LDLR and hnRNPD, hnRNPI or KHSRP, or the interaction of ZFP36L1 with the 3′-UTRs of PLK3 or VEGFA mRNAs (Supplementary Figure S2B). (ii) Oligo-L1 could stabilize LDLR mRNA in cells (Figure 3F, Supplementary Figure S3G, H and K). (iii) Oligo-L1 could increase the level of LDLR mRNA in cells (Figure 3D). (iv) Oligo-L1 could increase the level of LDLR protein in cells (Figure 3E and G, Supplementary Figure S3E and L). (v) Four control oligonucleotides, Oligo-L2, -L3, -L4, -L5 and -L6, could not inhibit the interaction between LDLR mRNA and ZFP36L1, and also could not increase the levels of LDLR mRNA or protein in cells (Figure 3D, E and G, Supplementary Figure S3E, J and L). These results indicate that the effect of Oligo-L1 is caused by disruption of the interaction between LDLR mRNA and ZFP36L1 and ZFP36L2. These results indicate that LNA-modified antisense oligonucleotides are a powerful tool for validating the function of RBPs. As Cibois *et al.* have also reported (27), antisense oligonucleotides allow us to elucidate the binding sites and the function of RNA/RBP interactions in cells.

In addition to validating the function of the interaction, we were able to increase the amount of LDLR protein in cells. In the liver, the LDLR binds to LDL, thereby lowering blood LDL levels. It has been reported that increasing the amount of LDLR protein in the liver could be a therapeutic approach for hyperlipidemia (28). Recently, some reports have shown that an anti-microRNA antisense oligonucleotide efficiently blocked the function of the microRNA, thereby alleviating diseases in rodents and nonhuman primates (29,30). These results demonstrate the potency of antisense oligonucleotide-based therapeutics. If appropriate delivery of Oligo-L1 to the liver could be achieved, this could result in a candidate drug for the treatment of hyperlipidemia. We believe that Oligo-L1 can be further developed to treat hyperlipidemia. However, it is also very important to consider off-target effects of antisense oligonucleotides, especially with regard to therapeutic applications.

Regulation of ZFP36L1

The CCR4-NOT poly (A) deadenylase complex is composed of more than 10 proteins, including CNOT7. It is known to interact with ZFP36 and ZFP36L1 and to act as an important effector complex of ZFP36-mediated mRNA-destabilization (16,17). We show in this report that PMA treatment causes dissociation of ZFP36L1 and CNOT7, and does not cause the dissociation of LDLR and ZFP36L1/L2 (Figure 4D). In the case of ZFP36L1, the interaction is somewhat increased by PMA treatment (Figure 4D, Supplementary Figure S5B); however, the mechanisms and meaning of enhanced PMA-mediated binding of ZFP36L1 to LDLR mRNA are still unknown. Recently, MAPKAPK2, a downstream kinase of p38, has been shown to phosphorylate ZFP36, but not in the C-terminal region, leading to dissociation of ZFP36 and CNOT7 (16,17). These findings indicate that ZFP36 family proteins are regulated by at least two independent signaling pathways. It is an open question, whether these pathways commonly regulate all ZFP36 family proteins or whether there are differences in regulation between ZFP36 family proteins. It will be important to investigate in detail the mechanisms of these regulatory pathways and to clarify their functional consequences.

SUPPLEMENTARY DATA

Supplementary Data are available at NAR Online.

ACKNOWLEDGMENTS

We thank Y Kawamura, N Goshima, K Shinya, S Chijiwa and T Tuchiura for providing reagents. We thank K Nakamura for excellent technical assistance. We also thank M Oubihi, T Hirose and K Horimoto for helpful discussions.

FUNDING

Galaxy Pharma Inc. Funding for open access charge: National Institute of Advanced Industrial Science and Technology.

Conflict of interest statement. None declared.

REFERENCES

1. Bakheet,T., Williams,B.R. and Khabar,K.S. (2006) ARED 3.0: the large and diverse AU-rich transcriptome. *Nucleic Acids Res.*, **34**, 111–114.
2. Barreau,C., Paillard,L. and Osborne,H.B. (2006) AU-rich elements and associated factors: are there unifying principles? *Nucleic Acids Res.*, **33**, 7138–7150.
3. Goa,G-W. and Mania,A. (2012) Low-density lipoprotein receptor (LDLR) family orchestrates cholesterol homeostasis. *Yale J. Biol. Med.*, **85**, 19–28.
4. Kong,W., Wei,J., Abidi,P., Lin,M., Inaba,S., Li,C., Wang,Y., Wang,Z., Si,S.,, Pan,H. *et al.* (2004) Berberine is a novel cholesterol-lowering drug working through a unique mechanism distinct from statins. *Nat. Med.*, **10**, 1344–1351.
5. Li,H., Chen,W., Zhou,Y., Abidi,P., Sharpe,O., Robinson,W.H., Kraemer,F.B. and Liu,J. (2009) Identification of mRNA binding proteins that regulate the stability of LDL receptor mRNA through AU-rich elements. *J. Lipid. Res.*, **50**, 820–831.
6. Sanduja,S., Blanco,F.F. and Dixon,D.A. (2011) The roles of TTP and BRF proteins in regulated mRNA decay. *Wiley Interdiscip. Rev. RNA*, **1**, 42–57.
7. Horner,T.J., Lai,W.S., Stumpo,D.J. and Blackshear,P.J. (2009) Stimulation of polo-like kinase 3 mRNA decay by tristetraprolin. *Mol. Cell. Biol.*, **29**, 1999–2010.
8. Hacker,C., Valchanova,R., Adams,S. and Munz,B. (2010) ZFP36L1 is regulated by growth factors and cytokines in keratinocytes and influences their VEGF production. *Growth Factors*, **28**, 178–190.
9. Kauppinen,S., Vester,B. and Wenge,J. (2005) Locked nucleic acid (LNA): high affinity targeting of RNA for diagnostics and therapeutics. *Drug Discov. Today*, **2**, 287–290.
10. Kourouklis,D., Murakami,H. and Suga,H. (2005) Programmable ribozymes for mischarging tRNA with nonnatural amino acids and their applications to translation. *Methods*, **36**, 239–244.
11. Iemura,S.I. and Natsume,T. (2012) One-by-one sample preparation method for protein network analysis. In Cai,J. (ed). *Protein Interaction*. Intech, Rijeka, Croatia, pp. 293–310.
12. Matsumoto,M., Oyamada,K., Takahashi,H., Sato,T., Hatakeyama,S. and Nakayama,K.I. (2009) Large-scale proteomic analysis of tyrosine- phosphorylation induced by T-cell receptor or B-cell receptor activation reveals new signaling pathways. *Proteomics*, **9**, 3549–3563.
13. Said,N., Rieder,R., Hurwitz,R., Deckert,J., Urlaub,H. and Vogel,J. (2009) In vivo expression and purification of aptamer-tagged small RNA regulators. *Nucleic Acids Res.*, **37**, e133.
14. Diribarne,G. and Bensaude,O. (2009) 7SK RNA, a non-coding RNA regulating P-TEFb, a general transcription factor. *RNA Biol.*, **6**, 122–128.
15. Seonmi,S., Yea,S.K., Jisu,K., Hyun-Mi,K., Dong-Eun,K. and Sang,S.H. (2013) Sniffing for gene-silencing efficiency of siRNAs in HeLa cells in comparison with that in HEK293T cells: correlation between knockdown efficiency and sustainability of siRNAs revealed by FRET-based probing. *Nucleic Acid Ther.*, **23**, 152–159.
16. Marchese,F.P., Aubareda,A., Tudor,C., Saklatvala,J., Clark,A.R. and Dean,J.L. (2010) MAPKAP kinase 2 blocks tristetraprolin-directed mRNA decay by inhibiting CAF1 deadenylase recruitment. *J. Biol. Chem.*, **285**, 27590–27600.
17. Sandler,H., Kreth,J., Timmers,H.T. and Stoecklin,G. (2011) Not1 mediates recruitment of the deadenylase Caf1 to mRNAs targeted for degradation by tristetraprolin. *Nucleic Acids Res.*, **10**, 4373–4386.
18. Hudson,B.P., Martinez-Yamout,M.A., Dyson,H.J. and Wright,P.E. (2004) Recognition of the mRNA AU-rich element by the zinc finger domain of TIS11d. *Nat. Struct. Mol. Biol.*, **11**, 257–264.
19. Duan,H., Cherradi,N., Feige,J.J. and Jefcoate,C. (2009) cAMP-dependent posttranscriptional regulation of steroidogenic acute regulatory (STAR) protein by the zinc finger protein ZFP36L1/TIS11b. *Mol. Endocrinol.*, **23**, 497–509.
20. Wassarman,D.A. and Steitz,J.A. (1991) Structural analyses of the 7SK ribonucleoprotein (RNP), the most abundant human small RNP of unknown function. *Mol. Cell. Biol.*, **11**, 3432–3445.
21. Yang,Z., Zhu,Q., Luo,K. and Zhou,Q. (2001) The 7SK small nuclear RNA inhibits the CDK9/cyclin T1 kinase to control transcription. *Nature*, **414**, 317–322.
22. Vasudevan,S. and Steitz,J.A. (2007) AU-rich-element-mediated upregulation of translation by FXR1 and Argonaute 2. *Cell*, **128**, 1105–1118.
23. Hogg,J.R. and Collins,K. (2007) RNA-based affinity purification reveals 7SK RNPs with distinct composition and regulation. *RNA*, **13**, 868–880.
24. Bessonov,S., Anokhina,M., Will,C.L., Urlaub,H. and Lührmann,R. (2008) Isolation of an active step I spliceosome and composition of its RNP core. *Nature*, **452**, 846–850.
25. Townley-Tilson,W.H., Pendergrass,S.A., Marzluff,W.F. and Whitfield,M.L. (2006) Genome-wide analysis of mRNAs bound to the histone stem-loop binding protein. *RNA*, **12**, 1853–1867.
26. Obika,S., Nanbu,D., Hari,Y., Andoh,J., Morio,K., Doi,T. and Imanishi,T. (1998) Stability and structural features of the duplexes containing nucleoside analogues with a fixed N-type conformation, 2′-O,4′-C-methyleneribonucleosides. *Tetrahedron Lett.*, **39**, 5401–5404.
27. Cibois,M., Gautier-Courteille,C., Vallée,A. and Paillard,L. (2010) A strategy to analyze the phenotypic consequences of inhibiting the association of an RNA-binding protein with a specific RNA. *RNA*, **16**, 10–15.
28. Garg,A. and Simha,V. (2007) Update on dyslipidemia. *J. Clin. Endocrinol. Metab.*, **92**, 1581–1589.
29. Elmén,J., Lindow,M., Schütz,S., Lawrence,M., Petri,A., Obad,S., Lindholm,M., Hedtjärn,M., Hansen,H.F., Berger,U. *et al.* (2008) LNA-mediated microRNA silencing in non-human primates. *Nature*, **452**, 896–899.
30. Lanford,R.E., Hildebrandt-Eriksen,E.S., Petri,A., Persson,R., Lindow,M., Munk,M.E., Kauppinen,S. and Ørum,H. (2010) Therapeutic silencing of microRNA-122 in primates with chronic hepatitis C virus infection. *Science*, **327**, 198–201.

THE JOURNAL OF BIOLOGICAL CHEMISTRY VOL. 289, NO. 37, pp. 25639–25654, September 12, 2014

Role of the ANKMY2-FKBP38 Axis in Regulation of the Sonic Hedgehog (Shh) Signaling Pathway*

Received for publication, February 14, 2014, and in revised form, July 28, 2014 Published, JBC Papers in Press, July 30, 2014, DOI 10.1074/jbc.M114.558635

Shotaro Saita[‡], Michiko Shirane[‡1], Tohru Ishitani[§], Nobuyuki Shimizu[§], and Keiichi I. Nakayama[‡]

From the [‡]Division of Cell Biology and [§]Division of Cell Regulation Systems, Medical Institute of Bioregulation, Kyushu University, 3-1-1 Maidashi, Higashi-ku, Fukuoka, Fukuoka 812-8582, Japan

Background: FK506-binding protein 38 (FKBP38) inhibits the Sonic hedgehog (Shh) signaling pathway in mouse embryos, but the underlying molecular mechanism has remained unclear.
Results: ANKMY2 interacts with FKBP38 and acts downstream of FKBP38 to activate Shh signaling.
Conclusion: The FKBP38-ANKMY2 axis plays a key role in regulation of Shh signaling *in vivo*.
Significance: Our findings reveal a new mode of regulation of the Shh pathway.

Sonic hedgehog (Shh) is a secreted morphogen that controls the patterning and growth of various tissues in the developing vertebrate embryo, including the central nervous system. Ablation of the FK506-binding protein 38 (FKBP38) gene results in activation of the Shh signaling pathway in mouse embryos, but the molecular mechanism by which FKBP38 suppresses Shh signaling has remained unclear. With the use of a proteomics approach, we have now identified ANKMY2, a protein with three ankyrin repeats and a MYND (myeloid, Nervy, and DEAF-1)-type Zn^{2+} finger domain, as a molecule that interacts with FKBP38. Co-immunoprecipitation analysis confirmed that endogenous FKBP38 and ANKMY2 interact in the mouse brain. Depletion or overexpression of ANKMY2 resulted in down- and up-regulation of Shh signaling, respectively, in mouse embryonic fibroblasts. Furthermore, combined depletion of both FKBP38 and ANKMY2 attenuated Shh signaling in these cells, suggesting that ANKMY2 acts downstream of FKBP38 to activate the Shh signaling pathway. Targeting of the zebrafish ortholog of mouse *Ankmy2* (*ankmy2a*) in fish embryos with an antisense morpholino oligonucleotide conferred a phenotype reflecting loss of function of the Shh pathway, suggesting that the regulation of Shh signaling by ANKMY2 is conserved between mammals and fish. Our findings thus indicate that the FKBP38-ANKMY2 axis plays a key role in regulation of Shh signaling *in vivo*.

The Sonic hedgehog (Shh) signaling pathway is conserved among animals and plays key roles in embryonic development, in the maintenance of adult stem cells, and in cancer (1–3). In the absence of Shh, the signaling pathway is inactivated as a result of inhibition of the seven-transmembrane domain protein Smoothened (Smo) by the membrane protein Patched (Ptch) (4). The pathway is activated by the binding of Shh to and the consequent inactivation of Ptch (5, 6), which relieves the inhibition of Smo. Active Smo then signals to the cytoplasm, resulting in activation of the zinc finger transcription factors that control the output of the Shh pathway, which in vertebrates are the Gli proteins (Gli1, -2, and -3) (7). A unique feature of the vertebrate Shh pathway is that the primary cilium plays a central role in signal transduction (8, 9), with the initial signaling events at the membrane taking place in this organelle. Ptch is located at the base of the primary cilium (10), and the binding of Shh to Ptch results in the activation of Smo and its recruitment to the cilium (11). By an as yet unknown mechanism, active Smo in the cilium relays the Shh signal to the cytoplasm, resulting in the activation of Gli2 and Gli3, which control transcription of Shh target genes, such as those for Gli1 and Ptch1 (7).

FKBP38 is a member of the FK506-binding protein (FKBP)[2] family (12, 13). It contains a transmembrane domain and a short juxtamembrane sequence at its COOH terminus, and it localizes predominantly to the mitochondrial outer membrane (14). We have previously shown that FKBP38 contributes to the localization of the antiapoptotic proteins Bcl-2 and Bcl-x_L to mitochondria and thereby inhibits apoptosis (15). FKBP38 translocates from mitochondria to the endoplasmic reticulum during mitophagy, with this translocation being essential for the suppression of apoptosis (16). In addition, FKBP38 appears to regulate protein degradation by anchoring the 26 S proteasome to organellar membranes (17). It thereby affects the stability of both Bcl-2 and the prolyl 4-hydroxylase domain-containing enzyme PHD2, the latter of which regulates the hypoxia-inducible transcription factor HIF1α (18). Although FKBP38 has been found to be expressed in all mammalian tissues examined, it is especially abundant in the central nervous system, both in neurons and in glial cells (19). To investigate the physiological roles of FKBP38, we generated mice nullizygous for the FKBP38 gene. We found that the *Fkbp38*$^{-/-}$ mice died shortly after birth, manifesting a defect in neural tube closure (spina bifida) (20), whereas others showed that FKBP38 controls neural tube patterning primarily by acting in a cell-autonomous manner to prevent inappropriate activation of the Shh

* This work was supported in part by a Japan Society for the Promotion of Science (JSPS) fellowship (to S. S.).
[1] To whom correspondence should be addressed: Dept. of Molecular and Cellular Biology, Medical Institute of Bioregulation, Kyushu University, 3-1-1 Maidashi, Higashi-ku, Fukuoka, Fukuoka 812-8582, Japan. Tel.: 81-92-642-6816; Fax: 81-92-642-6819; E-mail: smichi@bioreg.kyushu-u.ac.jp.

[2] The abbreviations used are: FKBP, FK506-binding protein; MEF, mouse embryonic fibroblast; MO, morpholino oligonucleotide; NTA, nitrilotriacetic acid; E11.5, embryonic day 11.5; hpf, hours postfertilization; EGFP, enhanced green fluorescent protein.

pathway by Gli2 (21). This role of FKBP38 is independent of the upstream pathway activator Smo but is dependent on the kinesin-2 motor subunit Kif3a, which participates in intraflagellar transport and cilium assembly.

We have now further investigated the physiological roles of FKBP38 by proteomic screening and thereby identified ANKMY2 (also known as ZMYND20) as a protein that interacts with FKBP38. Depletion or overexpression of ANKMY2 in mouse embryonic fibroblasts (MEFs) resulted in down- and up-regulation of Shh signaling, respectively. Our observation that depletion of both FKBP38 and ANKMY2 attenuated Shh signaling in these cells suggests that FKBP38 inhibits such signaling via suppression of the stimulatory effect of ANKMY2. Furthermore, the regulation of Shh signaling by ANKMY2 is conserved between mammals and fish, given that a morpholino oligonucleotide (MO) that targets the zebrafish ortholog of mouse *Ankmy2* (*ankmy2a*) conferred a specific phenotype reflecting loss of function of the Shh pathway in zebrafish embryos. We thus propose that the FKBP38-ANKMY2 axis plays a key role in regulation of the Shh signaling pathway *in vivo*.

EXPERIMENTAL PROCEDURES

Construction of Plasmids—Construction of vectors encoding human or mouse FKBP38 or human FKBP52 was described previously (15), and cDNAs encoding FKBP38 mutants were generated by PCR. Complementary DNAs encoding mouse Shh (full-length or amino acids 1–197) were generated by PCR with Prime Star polymerase (Takara, Ohtsu, Japan) from a brain cDNA library; those encoding human or mouse ANKMY2 (ZMYND20) were generated from human kidney and mouse brain cDNA libraries; those encoding mouse ZMYND1, -2, -3, -4, -7, -8, -12, -14, -15, -18, -19, -21, or -23 were generated from a mouse brain cDNA library; and those encoding human ZMYND5, -10, -11, or -17 were generated with the use of cDNA preparations from HeLa, SH-SY5Y, or HEK293T cells. Human ZMYND6 (PHD2) and mouse ZMYND9 (USP19) cDNAs were kindly provided by Y. Minamishima (Keio University, Japan) and S. S. Wing (McGill University, Montreal, Canada), respectively. Complementary DNAs encoding zebrafish ANKMY2a and FKBP38 were generated by PCR from a zebrafish cDNA library. For the production of recombinant proteins, the cDNA for mouse ANKMY2 was subcloned into pGEX-6P (GE Healthcare) and pET-28 (Novagen, Madison, WI), and that for mouse FKBP38 was subcloned into pET-28. Otherwise, cDNAs were subcloned into the p3×FLAG-CMV-7.1 (Sigma), pEF-BOS-2×HA (kindly provided by S. Nagata, Kyoto University), pcDNA3 (Invitrogen), pEGFP (Clontech), pCS2P+ (Addgene, Cambridge, MA), or pMX-puro (kindly provided by T. Kitamura, Tokyo University) vectors.

Cell Culture, Transfection, and Assay of Shh Signaling—Plat-E, HeLa, and HEK293T cells were maintained in DMEM supplemented with 10% FBS (Invitrogen) and, in the case of Plat-E cells, with blasticidin (10 μg/ml). Primary MEFs were isolated as described previously (22, 23) and were immortalized by transfection with a plasmid containing SV40 genomic DNA (kindly provided by T. Akagi, KAN Research Institute, Kobe, Japan). Retroviral infection was performed as described previously (24), and cells were transfected with expression vectors with the use of the FuGENE HD reagent (Invitrogen). Shh was produced in HEK293T cells by transient transfection of an expression plasmid encoding mouse Shh (amino acids 1–197) for 24 h, after which the medium was replaced with Opti-MEM reduced serum medium (Invitrogen), and the cells were incubated for an additional 24 h for collection of Shh-containing culture supernatants. For assay of Shh signaling, confluent cell cultures were deprived of serum for 24 h by incubation in Opti-MEM reduced serum medium, exposed to mouse Shh for the indicated times, and then harvested for RT and real-time PCR as well as immunoblot analyses.

RT and Real-time PCR Analysis of Shh Pathway Activity—Total RNA isolated from MEFs with the use of Isogen (Nippon Gene, Tokyo, Japan) was subjected to RT with the use of a QuantiTect reverse transcription kit (Qiagen, Hilden, Germany), and the resulting cDNA was subjected to PCR with Power SYBR Green PCR Master Mix in an ABI-Prism 7000 sequence detection system (Applied Biosystems, Foster City, CA). The amounts of each target mRNA were calculated and normalized by that of *Hprt* mRNA as described previously (25). The PCR primer sequences (sense and antisense, respectively) were 5′-ATCACCTGTTGGGGATGCTGGAT-3′ and 5′-GGCGTGAATAGGACTTCCGACAG-3′ for mouse *Gli1*, 5′-ACTGTCCAGCTACCCCAATG-3′ and 5′-CATCATGCCA-AAGAGCTCAA-3′ for mouse *Ptch1*, and 5′-GCCTAAGATG-AGCGCAAGTTG-3′ and 5′-TACATGGCAGATGGCCAC-AG-3′ for mouse *Hprt*.

RNAi—Stealth siRNAs targeted to mouse *Ankmy2* (*Ankmy2*-1, 5′-CCCAGGGACUGGAUAAAGAGCCAAA-3′; *Ankmy2*-2, 5′-CCACCCUGUCAAGAUCGUGAUGCUU-3′) or negative control duplexes (Invitrogen) were introduced into MEFs by reverse transfection with the use of Lipofectamine RNAiMax (Invitrogen).

Antibodies—Rabbit polyclonal antibodies to (anti-) FKBP38 (FK38N1) were generated in response to a hexahistidine (His_6)-tagged recombinant protein comprising the NH_2-terminal half of FKBP38 that was expressed in and purified from *Escherichia coli* (15). Rabbit polyclonal anti-ANKMY2 was generated in response to His_6-tagged recombinant full-length mouse ANKMY2 that was expressed in and purified from *E. coli*. Mouse monoclonal anti-HSP90 was obtained from BD Biosciences; rabbit polyclonal anti-calnexin was from Stressgen (Victoria, Canada); rabbit monoclonal anti-Gli1 (V812) was from Cell Signaling (Beverly, MA); anti-FLAG epitope (mouse monoclonal M2 and rabbit polyclonal), mouse monoclonal anti-acetylated α-tubulin, and anti-γ-tubulin were from Sigma; mouse monoclonal anti-HA epitope was from Research Diagnostics (Flanders, NJ); mouse monoclonal anti-GST (M071-3) was from MBL (Nagoya, Japan); and mouse monoclonal anti-T7 tag was from Novagen.

Generation of Transgenic Mice—Animal experiments were performed in accordance with the guidelines of Kyushu University. For generation of transgenic mouse lines, a cDNA for mouse FKBP38 tagged at its NH_2 terminus with His_6-FLAG was subcloned into the XhoI site of the pPrPpE1/E2, E3sal plasmid (26, 27). The resulting vector was digested with NotI for linearization and removal of the backbone vector. The prepared DNA construct was then injected into fertilized eggs of the

B6D2F1/Crlj (BDF1) background. Primary genotyping was performed by PCR and Southern blot analysis and was followed by immunoblot analysis with anti-FLAG. Examination of phenotypes was performed with mice of the C57BL/6J background. Wild-type (WT) littermates were studied as control mice.

Preparation of Protein Complexes by Dual Affinity Purification—Brains of mice stably expressing His_6-FLAG-tagged mouse FKBP38 were disrupted with a Potter homogenizer in a solution containing 10 mM Tris-HCl (pH 8.0), 0.32 M sucrose, 5 mM EDTA, 1 mM Na_3VO_4, 25 mM NaF, aprotinin (10 μg/ml), leupeptin (10 μg/ml), and 1 mM PMSF. The homogenate was centrifuged at 1000 × *g* for 5 min at 4 °C to remove nuclei and nondisrupted cells, and the resulting supernatant was centrifuged at 20,000 × *g* for 1 h at 4 °C to isolate a membrane fraction (pellet). This pellet was solubilized with a solution containing 20 mM Tris-HCl (pH 8.0), 150 mM NaCl, 1.0% Triton X-100, 1 mM Na_3VO_4, 25 mM NaF, aprotinin (10 μg/ml), leupeptin (10 μg/ml), and 0.5 mM PMSF, and the insoluble material was removed by centrifugation at 37,000 × *g* for 1 h at 4 °C. The protein concentration of the resulting supernatant was determined with the Bradford assay (Bio-Rad), and this soluble membrane fraction was then incubated with rotation for 1 h at 4 °C with 40 μl of anti-FLAG (M2)-agarose affinity gel (Sigma)/mg of protein. The beads were washed three times with solubilization buffer, after which protein complexes were eluted from the beads by incubation for several min at 4 °C with 800 μl of the same buffer containing the FLAG peptide (Sigma) at 0.25 mg/ml. For the second affinity purification step, nickel-nitrilotriacetic acid (Ni-NTA)-agarose (ProBond resin, Invitrogen) was added to the eluate at one-half the volume of anti-FLAG (M2)-agarose used in the first step, and the mixture was incubated with rotation for 1 h at 4 °C. The beads were washed three times with solubilization buffer, after which protein complexes were eluted by incubation for several min at 4 °C with the same solution containing 300 mM imidazole. Protein identification by LC-MS/MS analysis was performed as described previously (25).

Immunoprecipitation and Immunoblot Analysis—Whole mouse brain was homogenized by the application of 10 strokes (900 rpm) with a Potter homogenizer in a solution containing 20 mM HEPES-NaOH (pH 7.6), 0.32 M sucrose, 1 mM EDTA, 1 mM Na_3VO_4, 25 mM NaF, aprotinin (10 μg/ml), leupeptin (10 μg/ml), and 1 mM PMSF. The homogenate was centrifuged twice at 1000 × *g* for 5 min at 4 °C, and the second supernatant was centrifuged at 100,000 × *g* for 1 h at 4 °C. The crude microsomal pellet was resuspended in a lysis buffer (40 mM HEPES-NaOH (pH 7.5), 150 mM NaCl, 10% glycerol, 0.5% Triton X-100, 1 mM Na_3VO_4, 25 mM NaF, aprotinin (10 μg/ml), leupeptin (10 μg/ml), 1 mM PMSF), incubated for 1 h at 4 °C, and then centrifuged again at 100,000 × *g* for 1 h at 4 °C to remove insoluble material. The resulting supernatant was subjected to immunoprecipitation for 1 h at 4 °C with protein G-Sepharose 4 Fast Flow (Amersham Biosciences) and either anti-FKBP38, anti-ANKMY2, rabbit anti-FLAG, or normal rabbit serum. The immunoprecipitates were washed three times with lysis buffer and then subjected to immunoblot analysis, as described previously (28). The images were scanned with a LAS-4000 (GE Healthcare) instrument. For analysis of transfected HEK293T cells, the cells were cultured for 1 day after transfection and then lysed by incubation for 10 min at 4 °C with lysis buffer. The lysates were centrifuged at 20,400 × *g* for 10 min at 4 °C, after which equal amounts of protein from the resulting supernatants were subjected either to immunoblot analysis directly or to immunoprecipitation for 1 h at 4 °C with rabbit anti-FLAG and protein G-Sepharose 4 Fast Flow followed by immunoblot analysis.

In Vitro Binding Assay—Recombinant GST-ANKMY2 and His_6-T7-FKBP38 expressed in and purified from *E. coli* were mixed and then incubated at 4 °C for 1 h with rotation. After the addition of glutathione-Sepharose 4B beads (Amersham Biosciences), the mixture was incubated for an additional 1 h at 4 °C with rotation, the beads were washed twice, and the bound proteins were subjected to immunoblot analysis.

Immunofluorescence Analysis of Mouse Embryos—Mouse embryos at embryonic day 11.5 (E11.5) were fixed with 4% paraformaldehyde in PBS, exposed to 30% (w/v) sucrose in PBS, embedded in Tissue-Tek O.C.T. compound (Sakura, Tokyo, Japan), and cryosectioned at a thickness of 8 μm. Sections were rehydrated in PBS, permeabilized with 0.01% Triton X-100 in PBS containing 0.1% BSA, and incubated for 24 h at 4 °C with primary antibodies to ANKMY2. Immune complexes were detected with Alexa Fluor 488-conjugated goat secondary antibodies to rabbit IgG (Invitrogen) at a dilution of 1:500. Nuclei were stained with Hoechst 33258 (Wako, Osaka, Japan). Specimens were observed with a confocal microscope (LSM510 META, Carl Zeiss).

Immunofluorescence Analysis of Cells—HeLa cells grown on glass coverslips were transfected with the use of the FuGENE HD reagent and subsequently prepared for immunostaining. Confluent MEF cultures on glass coverslips were deprived of serum for 24 h by incubation in Opti-MEM reduced serum medium and subsequently prepared for immunostaining. In brief, cells were fixed for 10 min at room temperature with 4% formaldehyde in PBS and were then incubated for 2 h at room temperature first with primary antibodies in PBS containing 0.1% BSA and 0.1% saponin and then with Alexa Fluor 488- or Alexa Fluor 546-labeled goat secondary antibodies at a dilution of 1:2000. The cells were finally stained with Hoechst 33258, covered with a drop of GEL/MOUNT (Biomeda, Foster City, CA), and examined with a confocal microscope (LSM510 META) equipped with a ×63/1.4 oil immersion objective.

Injection of MOs—Antisense MOs (Gene Tools, Philomath, OR) were injected into zebrafish embryos at the one-cell stage according to standard protocols (29). Given that a high dose of MOs induces activation of the p53 pathway, we injected 2–5 ng of *ankmy2a* MO and 5 ng of *p53* MO concomitantly. The MO sequences were 5′-ACATTTCATTTCATTACCTCATCCA-3′ for *ankmy2a* spl MO, 5′-CTCCTTTCTTTGGTGCAGACATTAT-3′ for *ankmy2a* MO, and 5′-GCGCCATTGCTTTGCAAGAATTG-3′ for *p53* MO.

Cyclopamine Treatment—Cyclopamine (Sigma) was dissolved in DMSO. Early stage zebrafish embryos were manually dechorionated and treated with 10 nM cyclopamine (or 1% DMSO as a control) for 16 h in the dark at 28.5 °C.

In Situ Hybridization—Whole-mount zebrafish embryos were subjected to *in situ* hybridization under standard conditions with digoxigenin-labeled antisense RNA probes prepared from the zebrafish *ankmy2a* (FP102311, NM_199894), *gli1*

(CU855923, NM_178296), *myoD* (BX004812, NM_131262), *nkx2.2* (BX927409, NM_131422), or *fox2a* (CU856140, NM_001083815) genes.

Immunohistochemical Staining of Zebrafish Embryos—Immunohistochemical staining of zebrafish embryos was performed as described previously (30). Primary antibodies

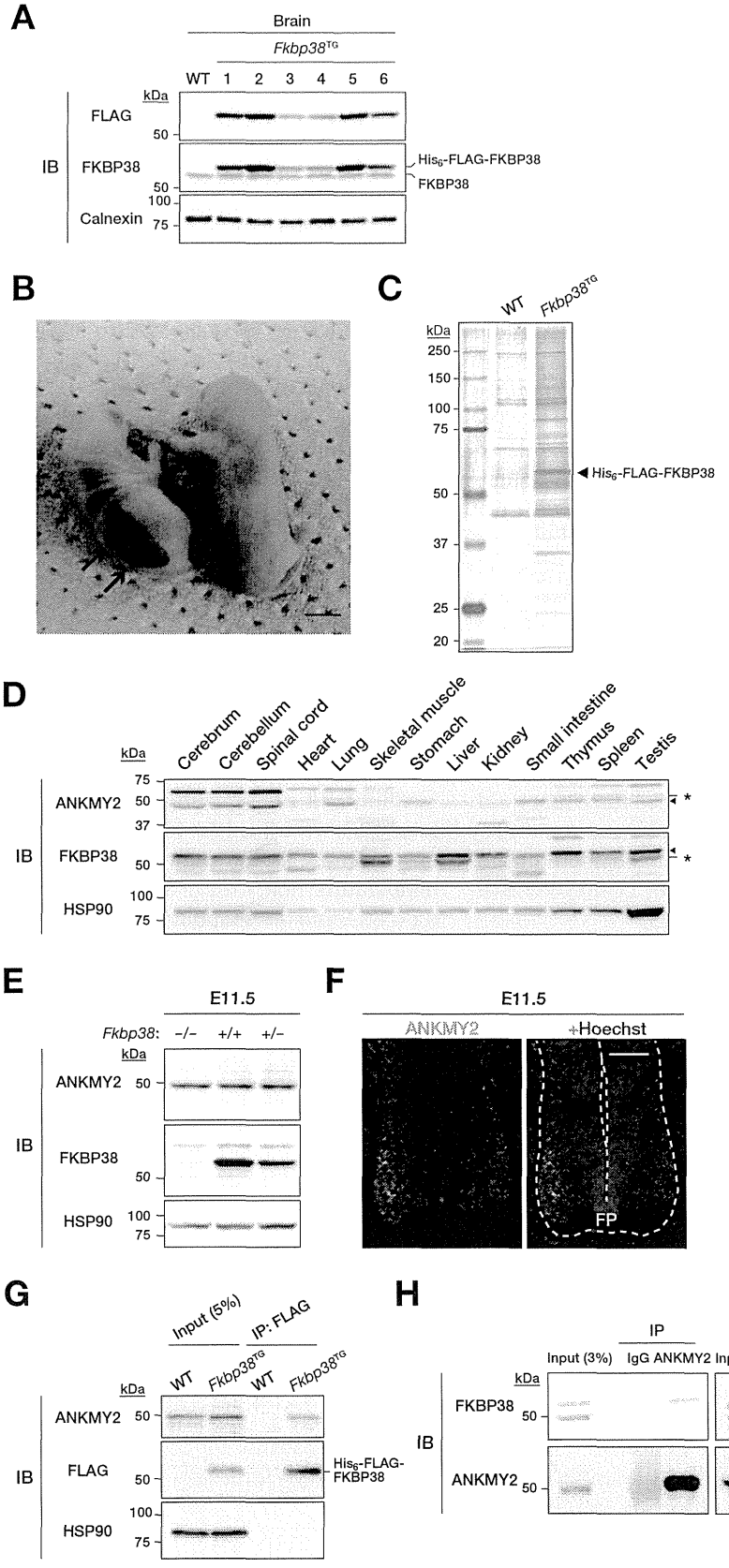

included F59, which preferentially recognizes slow muscle fibers (reacting only weakly with fast muscle fibers) (31), and 4D9, which recognizes zebrafish Engrailed (32), both of which were obtained from the Developmental Studies Hybridoma Bank (University of Iowa, Iowa City, IA). Immune complexes were detected with the use of HISTOFINE (Nichirei, Tokyo, Japan).

Statistical Analysis—Quantitative data are presented as means ± S.D. and were analyzed with Student's *t* test. A p value of <0.05 was considered statistically significant.

RESULTS

Identification of FKBP38-associated Proteins by a Proteomics Approach—To investigate the physiological roles of FKBP38, we adopted a proteomics approach to identify proteins with which FKBP38 is physically associated in neural cells of the brain. We thus generated mice (*Fkbp38*^{TG} mice) that express a transgene for FKBP38 tagged with His_6 and FLAG epitopes at its NH_2 terminus (His_6-FLAG-FKBP38) under the control of the neuron-specific prion gene promoter (26, 27). Expression of the transgene in the brain of six independent *Fkbp38*^{TG} lines was examined by immunoblot analysis (Fig. 1*A*). Animals of line 5 were chosen for most subsequent examinations because of their relatively high level of transgene expression. Spina bifida, the most prominent characteristic of newborn *Fkbp38*$^{-/-}$ mice, with a penetrance of 100% (20), was not observed in newborn *Fkbp38*$^{-/-}$ mice expressing the transgene (Fig. 1*B*), suggesting that His_6-FLAG-FKBP38 effectively substituted for endogenous FKBP38 in the brain. The *Fkbp38*$^{-/-;TG}$ mice died immediately after birth, however, indicating that neither the lack of FKBP38 in the brain nor the presence of spina bifida is primarily responsible for the neonatal death of *Fkbp38*$^{-/-}$ mice. Proteins associated with His_6-FLAG-FKBP38 were purified from lysates of the brain of *Fkbp38*^{TG} mice by dual affinity chromatography with anti-FLAG and Ni-NTA resin followed by SDS-PAGE and silver staining (Fig. 1*C*). The gel was then sliced, the gel fragments were exposed to trypsin, and the generated peptides were subjected to LC-MS/MS analysis. ANKMY2, a protein with three ankyrin repeats and a MYND (myeloid, Nervy, and DEAF-1)-type Zn^{2+} finger domain, showed the highest level of sequence coverage among the FKBP38-associated proteins identified by this approach (Table 1). We therefore compared the expression of ANKMY2 and FKBP38 in various mouse tissues. Immunoblot analysis revealed that ANKMY2 is highly expressed in the central nervous system, whereas FKBP38 is relatively widely distributed (Fig. 1*D*). Immunoblot analysis with anti-ANKMY2 also revealed that ANKMY2 was present in similar amounts regardless of FKBP38 abundance among *Fkbp38*$^{+/+}$, *Fkbp38*$^{+/-}$, and *Fkbp38*$^{-/-}$ mouse embryos at E11.5 (Fig. 1*E*). We also confirmed that ANKMY2 is expressed in the neural tube of mouse embryos at E11.5, being especially abundant in the ventral region near the floor plate that is under the influence of Shh signaling (Fig. 1*F*).

TABLE 1
Identification of FKBP38-associated proteins by proteomics analysis

Protein	Sequence coverage
	%
Ankyrin repeat- and MYND domain-containing protein 2 (ANKMY2)	21.1
T-complex protein 1, α subunit (TCPA)	11.3
T-complex protein 1, η subunit (TCPH)	2.9
T-complex protein 1, δ subunit (TCPD)	2.4

FKBP38 Specifically Interacts with ANKMY2—To confirm the interaction between FKBP38 and ANKMY2, we performed a co-immunoprecipitation assay with lysates prepared from the brains of WT or *Fkbp38*^{TG} mice. Immunoprecipitates prepared with anti-FLAG were subjected to immunoblot analysis with anti-FLAG and anti-ANKMY2 (Fig. 1*G*). ANKMY2 was detected in the immunoprecipitates prepared from *Fkbp38*^{TG} mouse brain lysates. Similar analysis was performed to detect the potential interaction between the two endogenous proteins. Immunoprecipitates prepared from WT mouse brain extract with anti-ANKMY2 were subjected to immunoblot analysis with anti-FKBP38. Endogenous FKBP38 was co-immunoprecipitated with endogenous ANKMY2 (Fig. 1*H*). A reciprocal experiment in which immunoprecipitates prepared with anti-FKBP38 were subjected to immunoblot analysis with anti-ANKMY2 also revealed that endogenous ANKMY2 interacted with endogenous FKBP38 (Fig. 1*H*). Collectively, these results suggested that FKBP38 interacts with ANKMY2 in the brain under physiological conditions.

We next examined the specificity of the interaction between FKBP38 and ANKMY2. We thus first determined whether ANKMY2 interacts with FKBP52, the FKBP family protein most closely related to FKBP38 (15, 33). A co-immunoprecipitation assay with transfected HEK293T cells revealed that, whereas FLAG-FKBP38 interacted with HA-ANKMY2, FLAG-FKBP52 did not (Fig. 2*A*), suggesting that the interaction between FKBP38 and ANKMY2 is specific. Furthermore, we investigated whether FKBP38 interacts with other members of the MYND-type Zn^{2+} finger protein family. Immunoblot anal-

FIGURE 1. **Identification of FKBP38-associated proteins by proteomics analysis of transgenic mice.** *A*, whole brain lysates prepared from WT or six different lines of *Fkbp38*^{TG} (harboring one allele of a His_6-FLAG-tagged FKBP38 transgene) mice were subjected to immunoblot (*IB*) analysis with anti-FLAG, anti-FKBP38, and anti-calnexin (loading control). *B*, gross appearance of newborns of *Fkbp38*$^{-/-}$ (*left*) and *Fkbp38*$^{-/-;TG}$ (*right*) mice. *Arrows*, neural tube closure defects; *arrowheads*, normal neural tube closure. *Scale bar*, 5 mm. *C*, extracts of WT or *Fkbp38*^{TG} mouse brain were subjected to dual affinity chromatography with anti-FLAG and Ni-NTA resin. The purified proteins were fractionated by SDS-PAGE and stained with silver. The *arrowhead* indicates the band corresponding to His_6-FLAG-FKBP38. *D*, immunoblot analysis of various mouse tissues with anti-ANKMY2, anti-FKBP38, and anti-HSP90 (loading control). *Asterisks*, nonspecific bands; *arrowheads*, corresponding specific bands. *E*, lysates prepared from *Fkbp38*$^{-/-}$, *Fkbp38*$^{+/+}$, and *Fkbp38*$^{+/-}$ mouse embryos (E11.5) were subjected to immunoblot analysis with anti-ANKMY2, anti-FKBP38, and anti-HSP90. *F*, immunohistofluorescence analysis of a neural tube section from a WT mouse embryo (E11.5) with anti-ANKMY2. Nuclei were stained with Hoechst 33258. *Dashed line*, neural tube. *FP*, floor plate. *Scale bar*, 100 μm. *G*, extracts of WT or *Fkbp38*^{TG} mouse brain were subjected to immunoprecipitation (*IP*) with anti-FLAG. The resulting precipitates, as well as a portion (5% of the input for immunoprecipitation) of the extracts, were subjected to immunoblot analysis with anti-ANKMY2, anti-FLAG, and anti-HSP90. *H*, WT mouse brain extract was subjected to immunoprecipitation with anti-ANKMY2, anti-FKBP38, or control rabbit IgG, after which the resulting precipitates, as well as a portion (3% of the input for immunoprecipitation) of the tissue extract, were subjected to immunoblot analysis with anti-FKBP38 and anti-ANKMY2. *Asterisk* and *arrowhead*, nonspecific and specific bands, respectively.

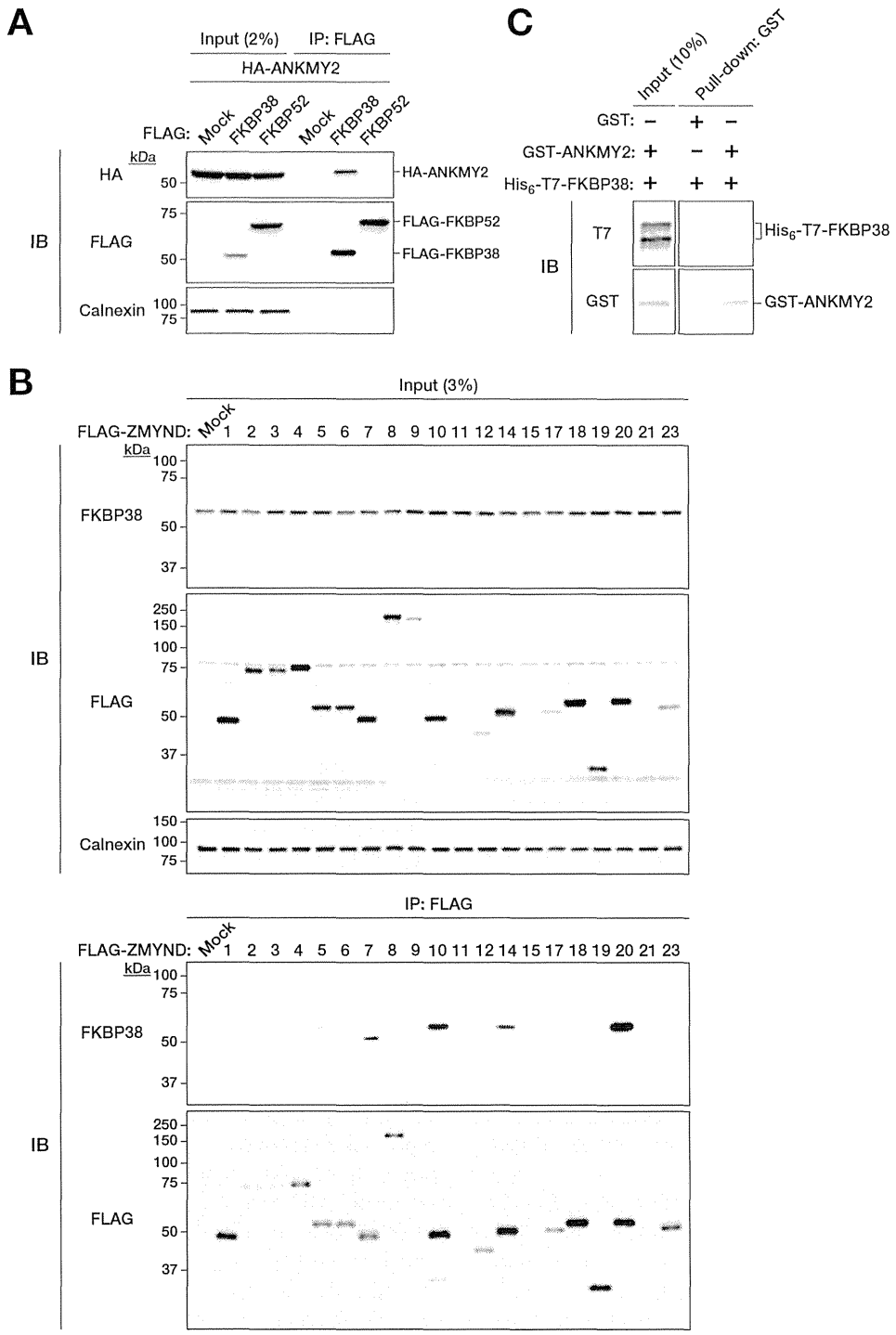

FIGURE 2. **Specificity of the interaction between FKBP38 and ANKMY2.** *A*, extracts of HEK293T cells transiently transfected with expression vectors for 3×FLAG-tagged human FKBP38 or human FKBP52 (*negative control*) and for 2×HA-tagged human ANKMY2 were subjected to immunoprecipitation with anti-FLAG. The resulting precipitates, as well as a portion (2% of the input for immunoprecipitation (*IP*)) of the cell extracts, were subjected to immunoblot analysis (*IB*) with anti-HA, anti-FLAG, and anti-calnexin. *B*, extracts of HEK293T cells transiently transfected with expression vectors for 3×FLAG-tagged ZMYND proteins were subjected to immunoprecipitation with anti-FLAG. The resulting precipitates, as well as a portion (3% of the input for immunoprecipitation) of the cell extracts, were subjected to immunoblot analysis with anti-FKBP38, anti-FLAG, and anti-calnexin. *C*, His_6-T7-tagged mouse FKBP38 was incubated with GST-tagged mouse ANKMY2 or GST (negative control), and the binding mixtures were then subjected to precipitation with glutathione-conjugated beads. The bead-bound proteins (pull-down), as well as a portion (10% of the input for precipitation) of the binding mixtures, were subjected to immunoblot analysis with anti-T7 and anti-GST.

ysis of immunoprecipitates prepared with anti-FLAG from lysates of HEK293T cells expressing 20 different FLAG-tagged MYND-type Zn^{2+} finger proteins revealed that ANKMY2 (ZMYND20) associated with endogenous FKBP38 to the greatest extent, whereas ZMYND7, ZMYND10, and ZMYND14 interacted with FKBP38 to a moderate extent (Fig. 2*B*). Although PHD2 (ZMYND6) was previously shown to interact with FKBP38 via its MYND domain (18), such interaction

occurred only at a low level, if at all, under our assay conditions. FLAG-tagged ZMYND11, -15, and -21 were expressed at only low levels in the transfected cells, possibly as a result of conformational constraints imposed by the FLAG tag or of instability of these proteins in HEK293T cells. Together, these results thus suggested that FKBP38 and ANKMY2 specifically associate with each other.

To examine whether FKBP38 and ANKMY2 directly bind to each other, we performed an *in vitro* pull-down assay with recombinant GST-tagged ANKMY2 and His_6-T7-tagged FKBP38 (Fig. 2*C*). GST-ANKMY2 bound to His_6-T7-FKBP38, whereas GST alone did not, indicating that FKBP38 and ANKMY2 indeed associate directly with each other.

Molecular Dissection of the FKBP38-ANKMY2 Interaction—Given that the NH_2 terminus of FKBP38 was shown to be necessary for interaction with PHD2 (ZMYND6) (18), we examined whether the binding of ANKMY2 to FKBP38 might also be dependent on this region of FKBP38. We constructed a mutant of human FKBP38 lacking 57 amino acids at the NH_2 terminus (Fig. 3*A*), and we found that the amount of endogenous ANKMY2 associated with this FKBP38(ΔN57) mutant in HEK293T cells was greatly reduced compared with that associated with the WT protein (Fig. 3*B*). This observation thus suggested that the interaction of FKBP38 with ANKMY2 is dependent on its NH_2-terminal domain.

ANKMY2 contains three ankyrin repeats, a MYND domain, and a coiled-coil domain (Fig. 3*C*). Given that FKBP38 interacted with not only ANKMY2 but also other related proteins harboring the MYND domain, we hypothesized that the MYND domain of ANKMY2 is required for interaction with FKBP38. To test this hypothesis, we generated a deletion mutant of mouse ANKMY2 that lacks the MYND domain (ΔMYND). Co-immunoprecipitation analysis revealed that this mutant was defective with regard to the ability to interact with FKBP38 (Fig. 3*D*). Given that the MYND domain contains two predicted Zn^{2+} finger motifs, we replaced amino acids required for the formation of these structures to generate W350A, C320S/C323S/C332S, C335S/C341S/C345S, and C357S mutants (Fig. 3*C*). None of these mutants associated with FKBP38 (Fig. 3*D*), suggesting that the integrity of the Zn^{2+} finger motifs of ANKMY2 is required for binding to FKBP38.

FKBP38 Inhibits Shh Signaling by Suppressing the Activity of ANKMY2—We next examined Shh signaling in MEFs derived from *Fkbp38*$^{+/+}$ or *Fkbp38*$^{-/-}$ embryos, given that FKBP38 has been implicated as a negative regulator of Shh signaling during development (21). The genes for Gli1 and Ptch1 are two early targets of Shh signaling, with the levels of the corresponding mRNAs and proteins increasing in a time-dependent manner (34). Confluent cultures of MEFs were deprived of serum for 24 h by incubation in Opti-MEM reduced serum medium and were then exposed to mouse Shh for assay of Shh signaling. Under this condition, we confirmed that both *Fkbp38*$^{+/+}$ and *Fkbp38*$^{-/-}$ MEFs possessed cilia with a basal body containing γ-tubulin and an axoneme containing acetylated α-tubulin (Fig. 4*A*). Treatment of *Fkbp38*$^{+/+}$ MEFs with Shh would be expected to activate the Shh pathway at Smo and thereby trigger downstream events that lead to up-regulation of *Gli1* expression. We found that the up-regulation of Gli1 protein by

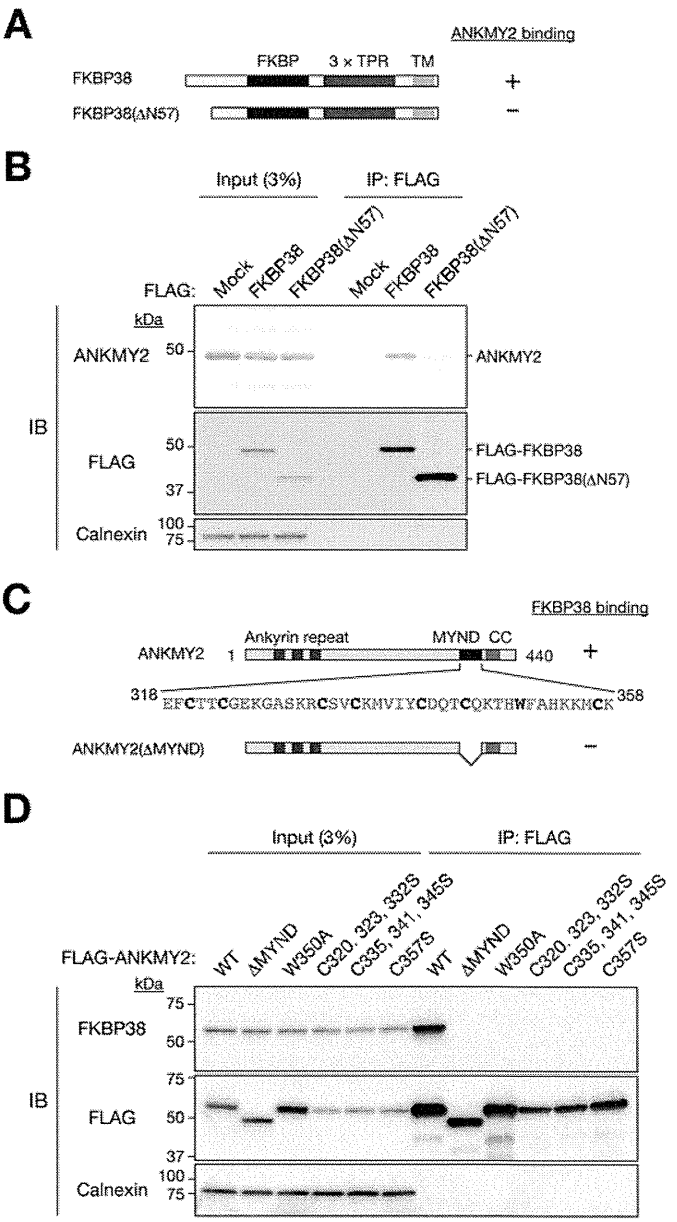

FIGURE 3. **Delineation of the regions of FKBP38 and ANKMY2 responsible for their interaction.** *A*, domain organization of human FKBP38 and structure of the FKBP38(ΔN57) mutant. *TPR*, tetratricopeptide repeat; *TM*, transmembrane. A summary of the ability of the WT and mutant proteins to bind ANKMY2 as determined in *B* is shown on the *right*. *B*, extracts of HEK293T cells transiently transfected with an expression vector for 3×FLAG-tagged human FKBP38 or FKBP38(ΔN57) were subjected to immunoprecipitation with anti-FLAG. The resulting precipitates, as well as a portion (3% of the input for immunoprecipitation (*IP*)) of the cell extracts, were subjected to immunoblot analysis with anti-ANKMY2, anti-FLAG, and anti-calnexin. *C*, domain organization of mouse ANKMY2 and structure of the ANKMY2(ΔMYND) mutant. *CC*, coiled-coil domain. A summary of the ability of the WT and mutant proteins to bind FKBP38 as determined in *D* is shown on the *right*. Individual residues of the MYND domain mutated in *D* are also indicated in *boldface type*. *D*, extracts of HEK293T cells transiently transfected with expression vectors for 3×FLAG-tagged WT or mutant forms of mouse ANKMY2 were subjected to immunoprecipitation with anti-FLAG. The resulting precipitates, as well as a portion (3% of the input for immunoprecipitation) of the cell extracts, were subjected to immunoblot analysis with anti-FKBP38, anti-FLAG, and anti-calnexin.

Shh was markedly more pronounced in *Fkbp38*$^{-/-}$ MEFs than in *Fkbp38*$^{+/+}$ MEFs (Fig. 4*B*). RT and real-time PCR analysis also showed that the amounts of *Gli1* and *Ptch1* mRNAs were increased by Shh to a significantly greater extent in *Fkbp38*$^{-/-}$

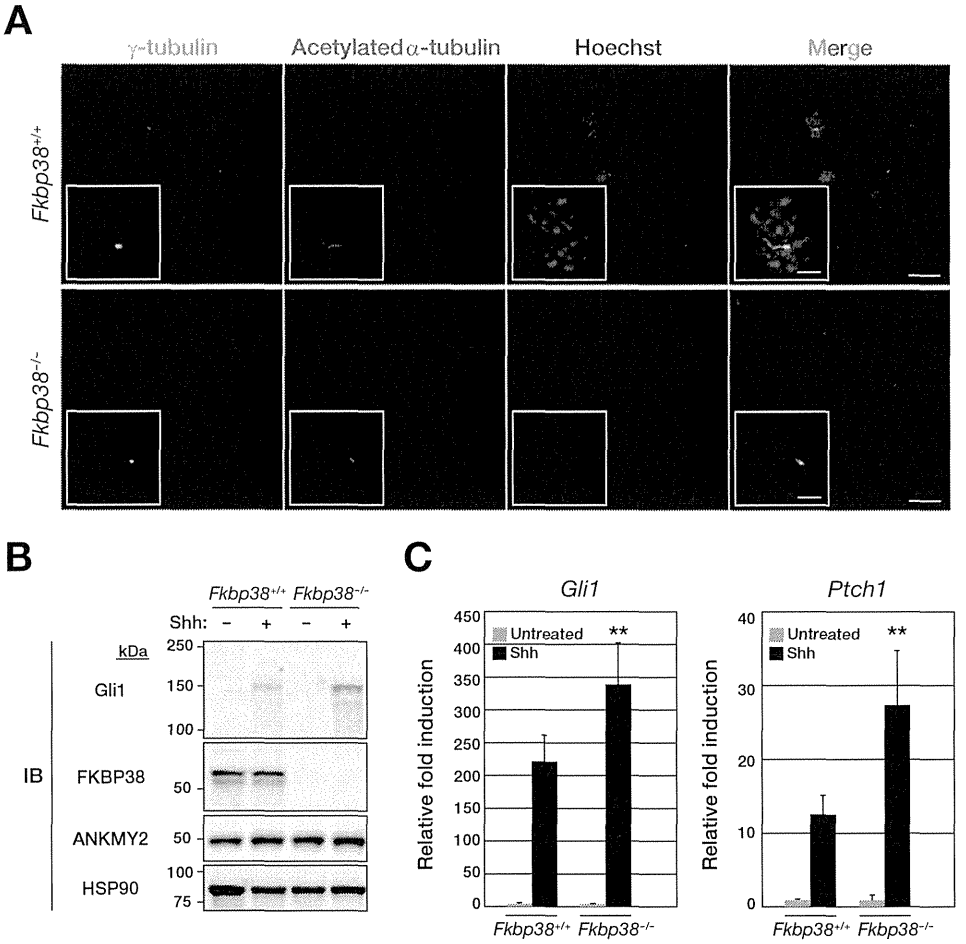

FIGURE 4. **FKBP38 is a negative regulator of Shh signal transduction.** *A*, confluent cultures of *Fkbp38*$^{+/+}$ or *Fkbp38*$^{-/-}$ MEFs that had been deprived of serum for 24 h by incubation in Opti-MEM reduced serum medium were fixed and processed for immunofluorescence analysis with antibodies to γ-tubulin and to acetylated α-tubulin. Nuclei were also stained with Hoechst 33258, and the cells were then examined with a confocal microscope. *Merged images* are also shown; *scale bars*, 20 μm. *Higher magnification views* are *boxed*; *scale bars*, 5 μm. *B*, *Fkbp38*$^{+/+}$ and *Fkbp38*$^{-/-}$ MEFs were incubated in the absence or presence of Shh for 48 h, after which whole cell homogenates were prepared and subjected to immunoblot analysis (*IB*) with anti-Gli1, anti-FKBP38, anti-ANKMY2, and anti-HSP90. *C*, *Fkbp38*$^{+/+}$ and *Fkbp38*$^{-/-}$ MEFs were incubated in the absence or presence of Shh for 24 h, after which total RNA was extracted from the cells and subjected to RT and real-time PCR analysis of *Gli1* and *Ptch1* mRNAs. Data are presented as relative -fold induction by Shh and are means ± S.D. from five independent experiments. **, $p < 0.01$ *versus* the corresponding value for *Fkbp38*$^{+/+}$ cells (Student's *t* test).

MEFs than in the WT cells (Fig. 4*C*). Together, these results were consistent with the notion that FKBP38 is a negative regulator of Shh signaling in mammalian cells.

ANKMY2 localizes to sensory cilia in *Caenorhabditis elegans*, with such localization being required for the proper ciliary localization of guanylyl cyclase (35, 36). Given that primary cilia are essential for signal transduction by the vertebrate Shh pathway (8, 9), we examined whether ANKMY2 functions as a regulator of Shh signaling in MEFs. Depletion of endogenous ANKMY2 mediated by two independent siRNAs attenuated the stimulatory effects of Shh on Gli1 expression at the protein (Fig. 5*A*) and mRNA (Fig. 5*B*) levels as well as on *Ptch1* mRNA abundance (Fig. 5*B*). Conversely, forced expression of ANKMY2 in MEFs enhanced these effects of Shh on *Gli1* and *Ptch1* expression (Fig. 5, *C* and *D*). Given that ANKMY2-(ΔMYND) also up-regulated the expression of *Gli1* and *Ptch1* to an extent similar to that observed with the WT protein (Fig. 5*D*), the MYND domain of ANKMY2 does not appear to be required for the activation of Shh signaling *per se*. We also examined the effects of forced expression of either WT or ΔN57 mutant forms of FKBP38 on Gli1 abundance in FKBP38-deficient MEFs. The up-regulation of Gli1 expression apparent in *Fkbp38*$^{-/-}$ MEFs compared with *Fkbp38*$^{+/+}$ cells was suppressed by forced expression of WT FKBP38 but not by that of FKBP38(ΔN57) (Fig. 5*E*), suggesting that the interaction of FKBP38 with ANKMY2 via the NH_2-terminal domain of the former protein is essential for the suppression of ANKMY2 function with regard to activation of Shh signaling. Together, these results indicated that FKBP38 and ANKMY2 are negative and positive regulators of mammalian Shh signaling, respectively.

We next examined how FKBP38 and ANKMY2 regulate Shh signaling by knockdown of ANKMY2 in FKBP38-deficient MEFs. Whereas FKBP38 deficiency enhanced the Shh-induced up-regulation of *Gli1* expression (Fig. 4), depletion of ANKMY2 in *Fkbp38*$^{-/-}$ MEFs reversed this effect at both the protein (Fig. 6*A*) and mRNA (Fig. 6*B*) levels. Similarly, whereas Shh-induced *Ptch1* transcription was enhanced in *Fkbp38*$^{-/-}$ MEFs compared with *Fkbp38*$^{+/+}$ MEFs (Fig. 4*C*), this difference was abolished by additional depletion of ANKMY2 (Fig.

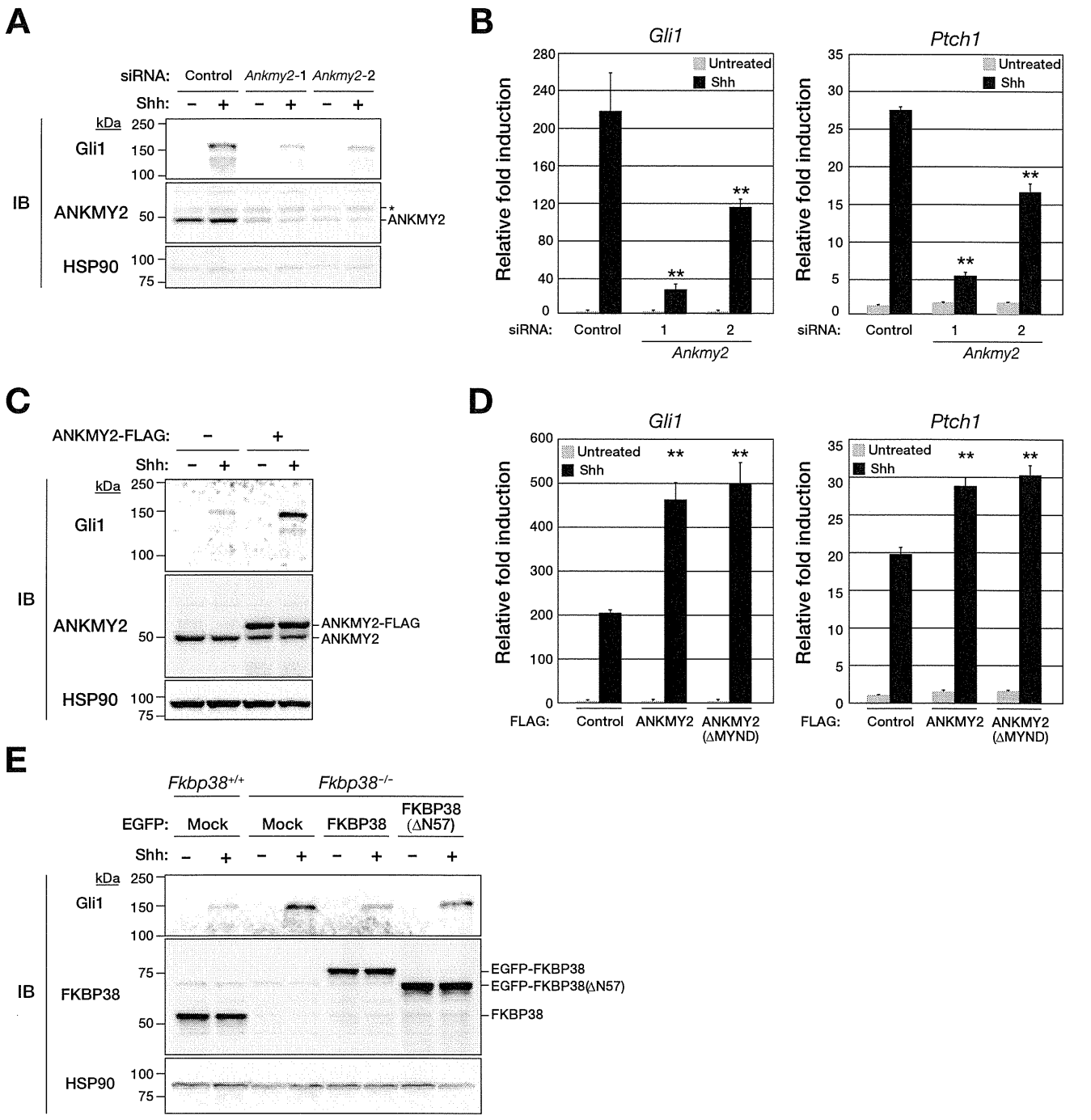

FIGURE 5. **ANKMY2 is a positive regulator of Shh signal transduction.** *A*, MEFs were transfected for 48 h with control or *Ankmy2* siRNAs and then incubated in the absence or presence of Shh for 48 h, after which whole cell homogenates were prepared and subjected to immunoblot analysis (*IB*) with anti-Gli1, anti-ANKMY2, and anti-HSP90. The *asterisk* indicates a nonspecific band. *B*, MEFs transfected with siRNAs as in *A* were incubated in the absence or presence of Shh for 24 h, after which total RNA was extracted from the cells and subjected to RT and real-time PCR analysis of *Gli1* and *Ptch1* mRNAs. Data are means ± S.D. (*error bars*) from three independent experiments. **, $p < 0.01$ *versus* the corresponding control value (Student's *t* test). *C*, MEFs stably expressing FLAG-tagged mouse ANKMY2 were incubated in the absence or presence of Shh for 48 h, after which whole cell homogenates were subjected to immunoblot analysis with anti-Gli1, anti-ANKMY2, and anti-HSP90. *D*, MEFs stably expressing FLAG-tagged ANKMY2 or ANKMY2(ΔMYND) were incubated in the absence or presence of Shh for 24 h and then subjected to RT and real-time PCR analysis of *Gli1* and *Ptch1* mRNAs. Data are means ± S.D. from three independent experiments. **, $p < 0.01$ *versus* the corresponding value for cells infected with the empty retrovirus (Student's *t* test). *E*, *Fkbp38*$^{+/+}$ or *Fkbp38*$^{-/-}$ MEFs stably expressing EGFP-tagged human FKBP38 or FKBP38(ΔN57) were incubated in the absence or presence of Shh for 48 h, after which whole cell homogenates were subjected to immunoblot analysis with anti-Gli1, anti-FKBP38, and anti-HSP90.

6*B*). This genetic evidence indicates that ANKMY2 is a downstream effector of FKBP38 (see Fig. 10). Specifically, our results suggested that FKBP38 is an upstream regulator that inhibits Shh signaling via suppression of the stimulatory activity of ANKMY2.

We also examined whether ANKMY2 overexpression might reverse the effect of FKBP38 overexpression on Shh target gene transcription in MEFs. The down-regulation of *Gli1* and *Ptch1* expression apparent in cells overexpressing FKBP38 was prevented by overexpression of ANKMY2 (Fig. 6*C*), again sug-

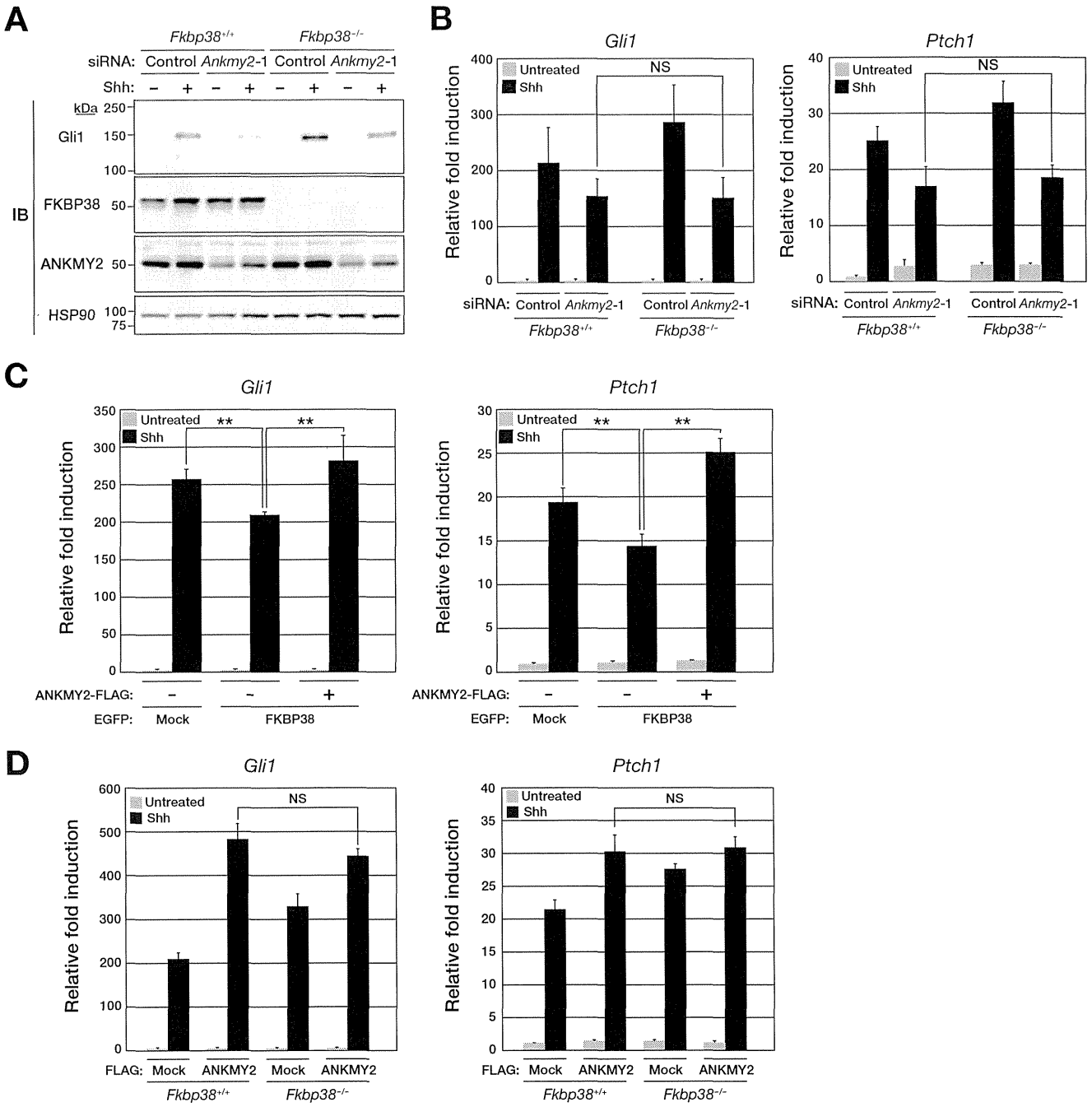

FIGURE 6. **FKBP38 inhibits Shh signaling via suppression of the stimulatory activity of ANKMY2.** *A*, *Fkbp38*$^{+/+}$ or *Fkbp38*$^{-/-}$ MEFs were transfected for 48 h with control or *Ankmy2* siRNAs and then incubated in the absence or presence of Shh for 48 h, after which whole cell homogenates were prepared and subjected to immunoblot analysis with anti-Gli1, anti-FKBP38, anti-ANKMY2, and anti-HSP90. *B*, *Fkbp38*$^{+/+}$ or *Fkbp38*$^{-/-}$ MEFs transfected with siRNAs as in *A* were incubated in the absence or presence of Shh for 24 h, after which total RNA was extracted from the cells and subjected to RT and real-time PCR analysis of *Gli1* (*left*) and *Ptch1* (*right*) mRNAs. *C*, MEFs stably expressing EGFP-tagged human FKBP38 and FLAG-tagged mouse ANKMY2, as indicated, were incubated in the absence or presence of Shh for 24 h, after which total RNA was extracted from the cells and subjected to RT and real-time PCR analysis of *Gli1* (*left*) and *Ptch1* (*right*) mRNAs. *D*, *Fkbp38*$^{+/+}$ or *Fkbp38*$^{-/-}$ MEFs stably expressing FLAG-tagged ANKMY2 were incubated in the absence or presence of Shh for 24 h, after which total RNA was extracted from the cells and subjected to RT and real-time PCR analysis of *Gli1* (*left*) and *Ptch1* (*right*) mRNAs. Data in *B–D* are means ± S.D. (*error bars*) from three independent experiments. **, $p < 0.01$ (Student's *t* test). *NS*, not significant.

gesting that FKBP38 antagonizes ANKMY2 function in the enhancement of Shh signaling. We also examined the effect of overexpression of ANKMY2 on *Gli1* and *Ptch1* expression in WT and FKBP38-deficient MEFs (Fig. 6*D*). Forced expression of ANKMY2 increased *Gli1* or *Ptch1* expression to similar levels in cells of both genotypes, suggesting that the observed levels of gene expression were maximal.

ANKMY2 Functions as a Positive Regulator of Shh Signaling in Vivo—We next sought to determine whether ANKMY2 is required for Shh signal transduction during embryogenesis in a living organism. Zebrafish possesses two paralogous *ankmy2* genes (*ankmy2a*, *ankmy2b*), probably as a result of a gene duplication event that occurred after its divergence from mammals. However, we were unable to detect *ankmy2b* mRNA in

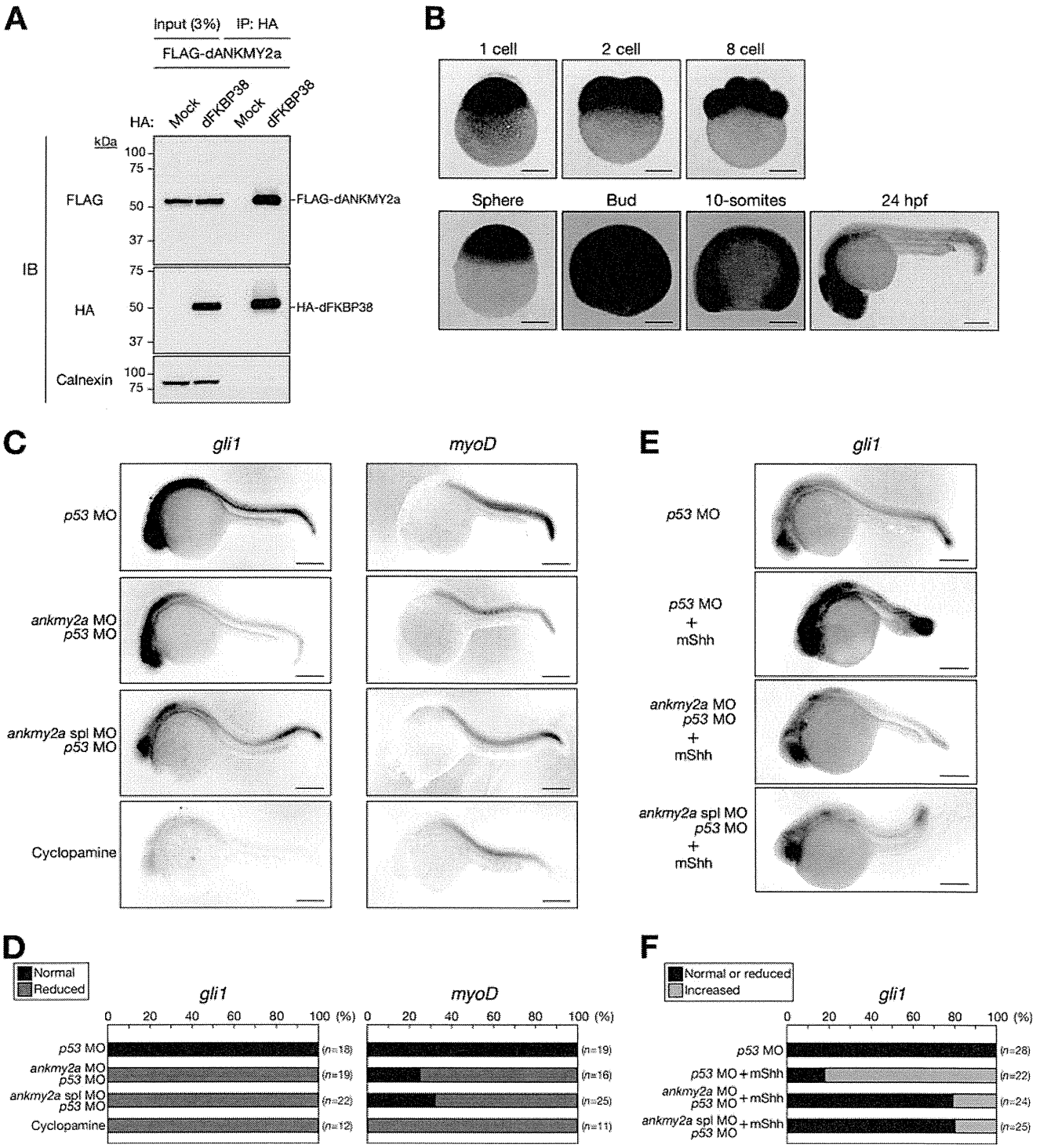

FIGURE 7. **Zebrafish *ankmy2a* expression is required for Shh signaling.** *A*, extracts of HEK293T cells transiently transfected with expression vectors for 3×FLAG-tagged dANKMY2a and for 2×HA-tagged dFKBP38 were subjected to immunoprecipitation (*IP*) with anti-HA. The resulting precipitates, as well as a portion (3% of the input for IP) of the cell extracts, were subjected to immunoblot analysis (*IB*) with anti-FLAG, anti-HA, and anti-calnexin. *B*, *in situ* hybridization of whole-mount zebrafish embryos at the indicated stages (hpf, hours postfertilization) with an antisense *ankmy2a* RNA probe. *C*, *in situ* hybridization of whole-mount zebrafish embryos at 24 hpf with antisense *gli1* or *myoD* RNA probes. The embryos had been injected with *ankmy2a* and *p53* antisense MOs at the one-cell stage or treated with cyclopamine, as indicated. *D*, percentages of embryos exhibiting normal or reduced *gli1* or *myoD* expression as determined in *C*. The *n* values correspond to the total numbers of embryos examined. *E*, *in situ* hybridization of whole-mount zebrafish embryos at 24 hpf with an antisense *gli1* RNA probe. The embryos had been injected with *ankmy2a* and *p53* antisense MOs in the absence or presence of mouse Shh (*mShh*) mRNA at the one-cell stage. *F*, percentages of embryos exhibiting normal or reduced *versus* increased *gli1* expression as determined in *E*. *Scale bars* (*B*, *C*, and *E*), 200 μm.

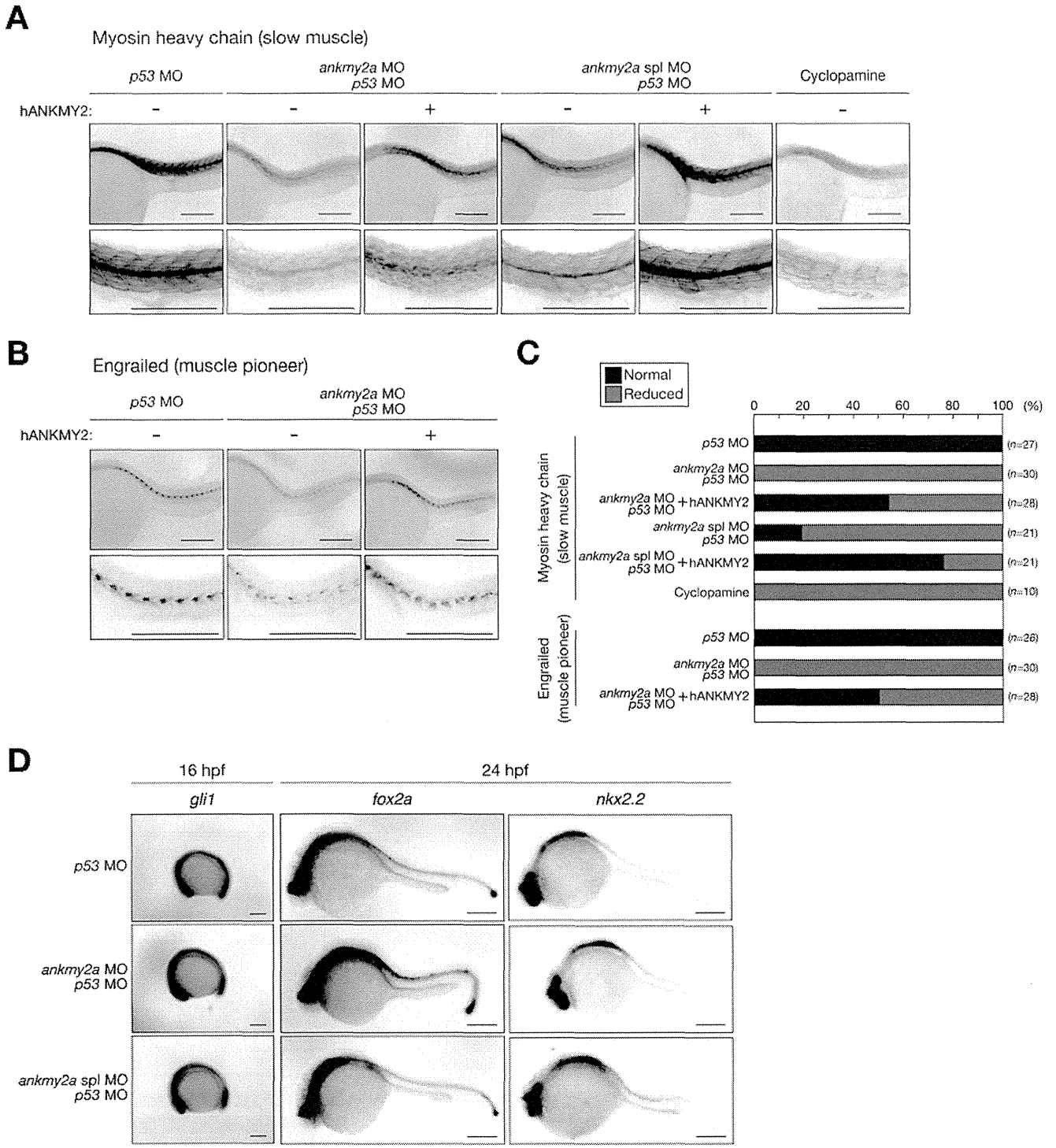

FIGURE 8. **Zebrafish *ankmy2a* expression is required for muscle development.** *A* and *B*, immunohistochemical staining of zebrafish embryos at 24 hpf with antibodies to myosin heavy chain (*A*) or to Engrailed (*B*). The embryos had been injected with *ankmy2a* and *p53* antisense MOs in the absence or presence of human ANKMY2 (*hANKMY2*) mRNA at the one-cell stage or treated with cyclopamine, as indicated. *C*, percentages of embryos exhibiting normal or reduced myosin heavy chain or Engrailed expression, as determined in *A* and *B*. The *n* values correspond to the total numbers of embryos examined. *D*, *in situ* hybridization of whole-mount zebrafish embryos at 16 or 24 hpf with antisense *gli1*, *fox2a*, or *nkx2.2* RNA probes. The embryos had been injected with *ankmy2a* and *p53* antisense MOs at the one-cell stage. *Scale bars* (*A*, *B*, *D*), 200 μm.

zebrafish by sensitive RT-PCR analysis (data not shown), suggesting that the gene is expressed at only a low level or not at all. To confirm the interaction between zebrafish FKBP38 and ANKMY2, we performed a co-immunoprecipitation assay. Immunoprecipitates were prepared with anti-HA from lysates of HEK293T cells transfected with expression vectors both for FLAG-tagged *Danio rerio* ANKMY2a (dANKMY2a) and for HA-tagged dFKBP38, and the resulting precipitates were subjected to immunoblot analysis with anti-HA and anti-FLAG (Fig. 7*A*). FLAG-dANKMY2a was detected in the immunopre-

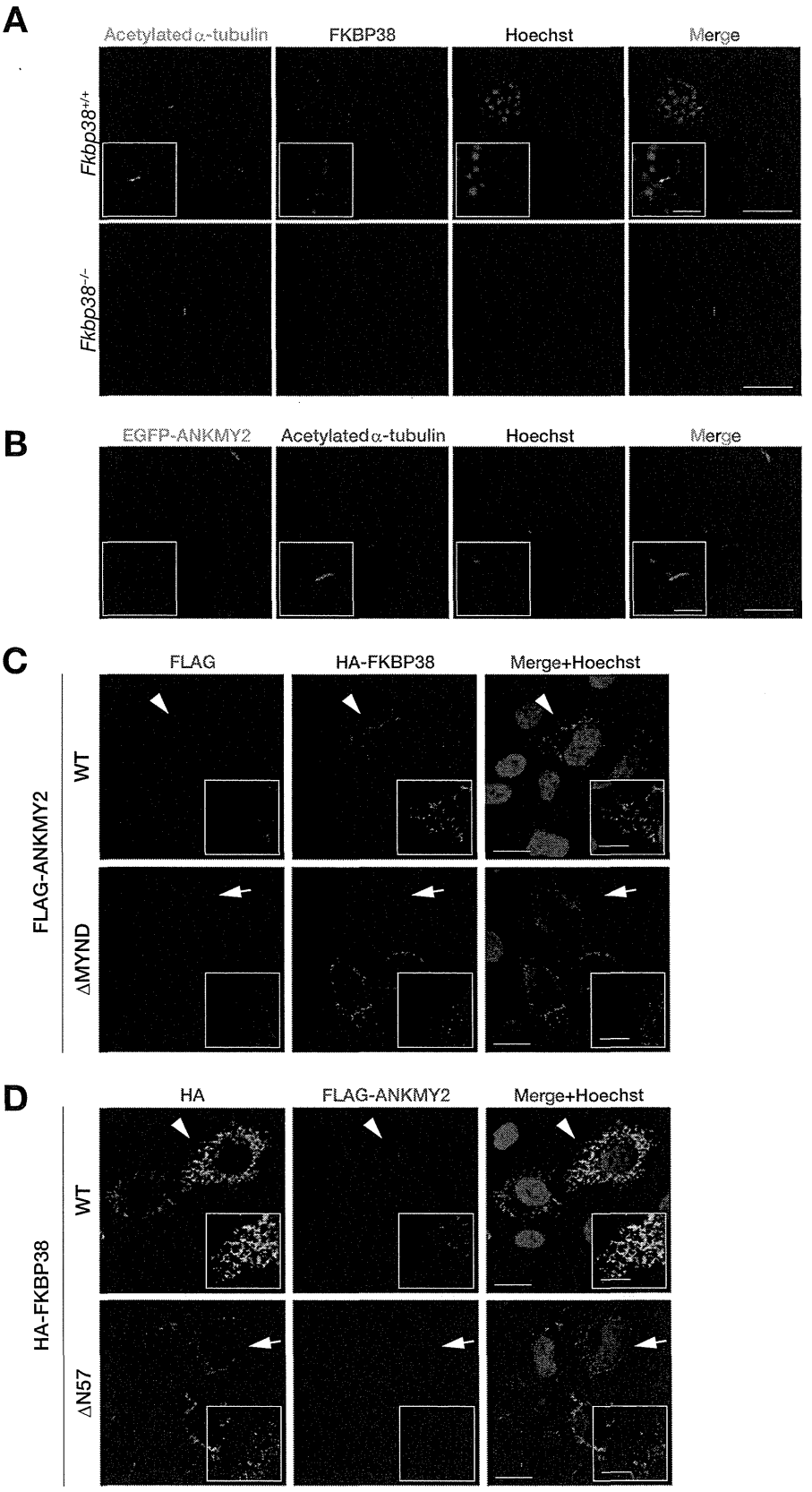

cipitates prepared from the cells expressing HA-dFKBP38, suggesting that the interaction of FKBP38 with ANKMY2 is conserved in zebrafish.

In situ hybridization revealed that *ankmy2a* is expressed in the neural tube of zebrafish embryos as early as the postsomitogenesis stage (Fig. 7*B*). We therefore investigated the functional role of dANKMY2a in Shh signaling. To this end, we inhibited the function of dANKMY2a with the use of antisense MOs, *ankmy2a* MO (for translational inhibition) or *ankmy2a* spl MO (for splicing inhibition). The Gli1 gene (*gli1*) is a target of the Shh pathway in fish and exhibits adaxial expression in normal embryos at 24 h postfertilization (hpf) (Fig. 7*C*). As a control, treatment of fish with cyclopamine, an inhibitor of the hedgehog signaling pathway, attenuated the expression of *gli1* (Fig. 7, *C* and *D*). Suppression of *ankmy2a* expression with antisense MOs resulted in down-regulation of the adaxial expression of *gli1* (Fig. 7, *C* and *D*), suggestive of reduced Shh signaling in the receiving cells. *In situ* hybridization analysis also revealed that the expression of *myoD*, a marker for muscle development, was attenuated by injection of *ankmy2a* antisense MOs or cyclopamine treatment (Fig. 7, *C* and *D*). We confirmed that the expression of *gli1* was enhanced by injection of embryos with mouse Shh mRNA (Fig. 7, *E* and *F*). Furthermore, this effect was reversed by co-injection of either *ankmy2a* MO or *ankmy2a* spl MO. Collectively, these results suggested that dANKMY2a is required for full activation of Shh signaling in zebrafish embryos.

Given that attenuation of Shh signaling was previously shown to impair the development of slow muscle in fish (37), we examined the effect of injection of *ankmy2a* antisense MOs on this process. Immunohistochemical staining for myosin heavy chain (expressed in slow muscle) and Engrailed (expressed in muscle pioneer cells, the anlagen of slow muscle), both of which are targets of Shh signaling, was indeed reduced by injection of either *ankmy2a* MO or *ankmy2a* spl MO (Fig. 8, *A–C*). This down-regulation of myosin heavy chain and Engrailed expression was prevented by co-injection of human ANKMY2 mRNA (Fig. 8, *A–C*), excluding the possibility of off-target effects of these antisense MOs and suggesting that the function of ANKMY2 is conserved from fish to humans. Collectively, these results suggested that dANKMY2a indeed contributes to slow muscle development and plays an integral role in activation of Shh signaling *in vivo*.

We also examined the effect of injection of *ankmy2a* MOs on dorsoventral patterning of the neural tube. We expected that the area expressing ventral markers in the neural tube might be reduced by suppression of *ankmy2a* expression. Unexpectedly, however, the expression patterns of *fox2a* and *nkx2.2* were unaffected by injection of either *ankmy2a* MO or *ankmy2a* spl MO (Fig. 8*D*). One possible explanation for these results is that dANKMY2a might be a context-dependent regulator rather than a universal activator of Shh signaling; it might thus influence *gli1* expression and slow muscle development but not dorsoventral patterning of the neural tube. Alternatively, given that muscle development begins at a relatively late stage of embryogenesis, whereas dorsoventral patterning of the neural tube occurs earlier at ~18 hpf, dANKMY2a might regulate Shh signaling only in the late phase of development in zebrafish Consistent with this notion, injection of *ankmy2a* MOs did not reduce the expression of *gli1* at 16 hpf (Fig. 8*D*) but did so at 24 hpf (Fig. 7, *C* and *D*).

FKBP38 Regulates ANKMY2 Localization—We next examined whether FKBP38 might affect the subcellular localization of ANKMY2, given that FKBP38 contributes to the mitochondrial localization of Bcl-2 and Bcl-x_L (15). We thus determined the subcellular localization of endogenous FKBP38 and EGFP-tagged ANKMY2 in MEFs with a primary cilium, a sensor for Shh. We found that FKBP38 was localized predominantly to mitochondria, with no apparent localization to cilia (Fig. 9*A*). Whereas ANKMY2 was previously shown to localize to cilia in *C. elegans* (35, 36), we found that EGFP-ANKMY2 was distributed throughout the cytoplasm of MEFs, with no apparent localization to cilia (Fig. 9*B*). This discrepancy is probably attributable to the difference in cell type or species studied. We speculate that a small but undetectable amount of ANKMY2 is present at cilia and that this fraction is reduced by sequestration of the protein from cilia to mitochondria mediated by the interaction with FKBP38. Consistent with this hypothesis, forced expression of HA-FKBP38 resulted in the apparent redistribution of FLAG-ANKMY2 from the cytoplasm to mitochondria, whereas it did not affect the localization of FLAG-ANKMY2(ΔMYND), which is not able to interact with FKBP38 (Fig. 9*C*). We also found that HA-FKBP38(ΔN57), which is not able to interact with ANKMY2 or to suppress its function, also did not affect the localization of FLAG-ANKMY2 (Fig. 9*D*). Together, these results revealed a correlation between the localization of ANKMY2 and its function in activation of Shh signaling, suggesting that FKBP38 probably regulates the function of ANKMY2 by controlling its localization through interaction with this protein.

FIGURE 9. **FKBP38 regulates ANKMY2 localization.** *A*, confluent cultures of *Fkbp38*$^{+/+}$ or *Fkbp38*$^{-/-}$ MEFs that had been deprived of serum for 24 h by incubation in Opti-MEM reduced serum medium were fixed and processed for immunofluorescence analysis with antibodies to acetylated α-tubulin and to FKBP38. Nuclei were stained with Hoechst 33258, and the cells were then examined with a confocal microscope. *Merged images* are also shown; *scale bars*, 20 μm. *Higher magnification views* are *boxed*; *scale bar*, 5 μm. *B*, confluent cultures of MEFs stably expressing EGFP-tagged human ANKMY2 were deprived of serum for 24 h, fixed, and processed for immunofluorescence analysis with antibodies to acetylated α-tubulin. Nuclei were stained with Hoechst 33258, and the cells were then examined with a confocal microscope. The fluorescence of EGFP-ANKMY2 was monitored directly. A *merged image* is also shown; *scale bar*, 20 μm. *Higher magnification* views are *boxed*; *scale bar*, 5 μm. *C*, HeLa cells expressing 2×HA-tagged human FKBP38 and 3×FLAG-tagged mouse ANKMY2 or ANKMY2(ΔMYND) were fixed and processed for immunofluorescence staining with anti-FLAG and anti-HA. Nuclei were stained with Hoechst 33258, and the cells were then examined with a confocal microscope. *Merged images* are also shown; *scale bars*, 20 μm. *Higher magnification* views are *boxed*; *scale bars*, 10 μm. An *arrowhead* indicates colocalization of ANKMY2 and FKBP38 signals; an *arrow* indicates that ANKMY2(ΔMYND) and FKBP38 signals are not colocalized. *D*, HeLa cells expressing 3×FLAG-tagged ANKMY2 and 2×HA-tagged FKBP38 or FKBP38(ΔN57) were fixed and processed for immunofluorescence staining with anti-HA and anti-FLAG. Nuclei were stained with Hoechst 33258, and the cells were then examined with a confocal microscope. *Merged images* are also shown; *scale bars*, 20 μm. *Higher magnification views* are *boxed*; *scale bars*, 10 μm. An *arrowhead* indicates colocalization of ANKMY2 and FKBP38 signals; an *arrow* indicates that ANKMY2 and FKBP38(ΔN57) signals are not colocalized.

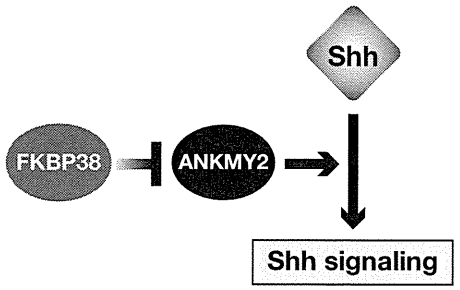

FIGURE 10. **Model for FKBP38-mediated regulation of Shh signaling.** FKBP38 regulates Shh signaling by suppression of ANKMY2 function. Loss of FKBP38 results in the activation of ANKMY2 and enhanced Shh signaling, leading to aberrant neural tube development.

DISCUSSION

Although the phenotypes associated with FKBP38 ablation in mice suggested that FKBP38 suppresses Shh signaling during development, the detailed mechanism by which FKBP38 inhibits such signaling had remained unclear. To explore this mechanism, we applied a dual affinity purification system to FKBP38 tagged with His_6 and FLAG epitopes and expressed in the brain of transgenic mice. This system allowed us to identify physiological targets of FKBP38 *in vivo*, with ANKMY2 being the target with the highest sequence coverage. Co-immunoprecipitation analysis further revealed that the MYND domain of ANKMY2 interacts with the NH_2-terminal domain of FKBP38. Although PHD2 (ZMYND6), another MYND-type Zn^{2+} finger protein, was previously shown to interact with FKBP38 (18), we found that the extent of this interaction was minimal compared with that between FKBP38 and ANKMY2 (ZMYND20). Our finding that the MYND-type Zn^{2+} finger domain of ANKMY2 is responsible for binding to FKBP38 suggests that other proteins with this type of domain might also associate with FKBP38. Indeed, we found that ZMYND7, -10, and -14 also interacted with FKBP38, although the physiological roles of these interactions remain unknown.

We have shown that ANKMY2 is a positive regulator of Shh signaling and that FKBP38 is an upstream regulator that inhibits Shh signaling by abrogation of the function of ANKMY2 (Fig. 10). The mechanisms by which ANKMY2 enhances Shh signaling and by which FKBP38 antagonizes this action of ANKMY2 remain unclear, however. ANKMY2 localizes to cilia and contributes to the intraflagellar transport-independent translocation of guanylyl cyclase in *C. elegans* (35, 36). We confirmed the interaction between ANKMY2 and guanylyl cyclase in mammalian cells (data not shown). In this regard, it is of note that cGMP activates Shh signaling in mammals (38). Given that protein kinase G (PKG) activated by cGMP phosphorylates Gli3, resulting in activation of Shh signaling (39), it is possible that the FKBP38-ANKMY2 axis controls Shh signaling via the cGMP-PKG pathway.

One of the molecular functions of FKBP38 is recruitment of its interacting proteins, such as Bcl-2 and Bcl-x_L, to the mitochondrial outer membrane. Overexpression of FKBP38 blocks apoptosis as a result of enhanced recruitment of Bcl-2 and Bcl-x_L to mitochondria, whereas depletion of FKBP38 results in mislocalization of these proteins (15). Similarly, we found that overexpression of FKBP38 in mammalian cells triggered translocation of ANKMY2 to mitochondria. Such translocation of ANKMY2 induced by FKBP38 might be responsible for the abrogation of putative ANKMY2 function that contributes to the activation of guanylyl cyclase in cilia. This hypothesis remains to be tested in the future.

Acknowledgments—We thank Y. Minamishima, S. S. Wing, S. Nagata, T. Kitamura, and T. Akagi for providing vectors and DNA; K. Tsunematsu and other laboratory members for technical assistance; and A. Ohta for help in preparation of the manuscript.

REFERENCES

1. Huangfu, D., and Anderson, K. V. (2005) Cilia and Hedgehog responsiveness in the mouse. *Proc. Natl. Acad. Sci. U.S.A.* **102,** 11325–11330
2. Lum, L., and Beachy, P. A. (2004) The Hedgehog response network: sensors, switches, and routers. *Science* **304,** 1755–1759
3. Rohatgi, R., and Scott, M. P. (2007) Patching the gaps in Hedgehog signalling. *Nat. Cell Biol.* **9,** 1005–1009
4. Alcedo, J., Ayzenzon, M., Von Ohlen, T., Noll, M., and Hooper, J. E. (1996) The *Drosophila* smoothened gene encodes a seven-pass membrane protein, a putative receptor for the hedgehog signal. *Cell* **86,** 221–232
5. Marigo, V., Davey, R. A., Zuo, Y., Cunningham, J. M., and Tabin, C. J. (1996) Biochemical evidence that patched is the Hedgehog receptor. *Nature* **384,** 176–179
6. Stone, D. M., Hynes, M., Armanini, M., Swanson, T. A., Gu, Q., Johnson, R. L., Scott, M. P., Pennica, D., Goddard, A., Phillips, H., Noll, M., Hooper, J. E., de Sauvage, F., and Rosenthal, A. (1996) The tumour-suppressor gene patched encodes a candidate receptor for Sonic hedgehog. *Nature* **384,** 129–134
7. Hui, C. C., and Angers, S. (2011) Gli proteins in development and disease. *Annu. Rev. Cell Dev. Biol.* **27,** 513–537
8. Murdoch, J. N., and Copp, A. J. (2010) The relationship between sonic Hedgehog signaling, cilia, and neural tube defects. *Birth Defects Res. A Clin. Mol. Teratol.* **88,** 633–652
9. Fliegauf, M., Benzing, T., and Omran, H. (2007) When cilia go bad: cilia defects and ciliopathies. *Nat. Rev. Mol. Cell Biol.* **8,** 880–893
10. Rohatgi, R., Milenkovic, L., and Scott, M. P. (2007) Patched1 regulates hedgehog signaling at the primary cilium. *Science* **317,** 372–376
11. Corbit, K. C., Aanstad, P., Singla, V., Norman, A. R., Stainier, D. Y., and Reiter, J. F. (2005) Vertebrate Smoothened functions at the primary cilium. *Nature* **437,** 1018–1021
12. Barik, S. (2006) Immunophilins: for the love of proteins. *Cell. Mol. Life Sci.* **63,** 2889–2900
13. Hamilton, G. S., and Steiner, J. P. (1998) Immunophilins: beyond immunosuppression. *J. Med. Chem.* **41,** 5119–5143
14. Lam, E., Martin, M., and Wiederrecht, G. (1995) Isolation of a cDNA encoding a novel human FK506-binding protein homolog containing leucine zipper and tetratricopeptide repeat motifs. *Gene* **160,** 297–302
15. Shirane, M., and Nakayama, K. I. (2003) Inherent calcineurin inhibitor FKBP38 targets Bcl-2 to mitochondria and inhibits apoptosis. *Nat. Cell Biol.* **5,** 28–37
16. Saita, S., Shirane, M., and Nakayama, K. I. (2013) Selective escape of proteins from the mitochondria during mitophagy. *Nat. Commun.* **4,** 1410
17. Nakagawa, T., Shirane, M., Iemura, S., Natsume, T., and Nakayama, K. I. (2007) Anchoring of the 26S proteasome to the organellar membrane by FKBP38. *Genes Cells* **12,** 709–719
18. Barth, S., Edlich, F., Berchner-Pfannschmidt, U., Gneuss, S., Jahreis, G., Hasgall, P. A., Fandrey, J., Wenger, R. H., and Camenisch, G. (2009) Hypoxia-inducible factor prolyl-4-hydroxylase PHD2 protein abundance depends on integral membrane anchoring of FKBP38. *J. Biol. Chem.* **284,** 23046–23058
19. Nielsen, J. V., Mitchelmore, C., Pedersen, K. M., Kjaerulff, K. M., Finsen, B., and Jensen, N. A. (2004) Fkbp8: novel isoforms, genomic organization, and characterization of a forebrain promoter in transgenic mice. *Genomics* **83,** 181–192